



**HAL**  
open science

# A Cretaceous pole from south China, and the Mesozoic hairpin turn of the Eurasian apparent polar wander path

Randolph Enkin, Yan Chen, Vincent Courtillot, Jean Besse, Lisheng Xing,  
Zhenhai Zhang, Zhonghai Zhuang, Jingxin Zhang

## ► To cite this version:

Randolph Enkin, Yan Chen, Vincent Courtillot, Jean Besse, Lisheng Xing, et al.. A Cretaceous pole from south China, and the Mesozoic hairpin turn of the Eurasian apparent polar wander path. *Journal of Geophysical Research: Solid Earth*, 1991, 96 (B3), pp.4007-4027. 10.1029/90JB01904 . insu-03655522

**HAL Id: insu-03655522**

**<https://insu.hal.science/insu-03655522>**

Submitted on 29 Apr 2022

**HAL** is a multi-disciplinary open access archive for the deposit and dissemination of scientific research documents, whether they are published or not. The documents may come from teaching and research institutions in France or abroad, or from public or private research centers.

L'archive ouverte pluridisciplinaire **HAL**, est destinée au dépôt et à la diffusion de documents scientifiques de niveau recherche, publiés ou non, émanant des établissements d'enseignement et de recherche français ou étrangers, des laboratoires publics ou privés.

Copyright

# A Cretaceous Pole From South China, and the Mesozoic Hairpin Turn of the Eurasian Apparent Polar Wander Path

RANDOLPH J. ENKIN,<sup>1</sup> YAN CHEN, VINCENT COURTILOT, AND JEAN BESSE

*Institut de Physique du Globe de Paris*

LISHENG XING, ZHENHAI ZHANG, ZHONGHAI ZHUANG, JINGXIN ZHANG

*Chinese Academy of Geological Sciences, Beijing*

To contribute to the apparent polar wander path (APWP) of the South China Block and Eurasia in general, we collected paleomagnetic samples from Mesozoic red beds around the city of Ya'an (30°N, 103°E) in the western tip of the Sichuan Basin. In this paper we present the results from 373 oriented cores taken from one section representing 3 km of sedimentary rocks. The section is dated with continental ostracods and with a magnetostratigraphic correlation between a densely sampled 272-m sequence and the polarity time scale, giving an upper Jurassic to Upper Cretaceous or Lower Tertiary age. The remanent direction is remarkably stable throughout the section ( $D=2.0^\circ$ ,  $I=34.2^\circ$ ,  $k=63.1$ ,  $\alpha_{95}=3.6^\circ$ ,  $N=26/28$  sites). While this fact might suggest that the section has been remagnetized, paleomagnetic and rock magnetic tests indicate that the remanence is primary. The pole position (78.6°N, 273.4°E,  $dp=2.4^\circ$ ,  $dm=4.1^\circ$ ) corresponds to a rather low paleolatitude ( $\lambda=18.8^\circ\pm 2.4^\circ$ ) but is consistent with other Cretaceous poles from China. If one accepts the Eurasian APWP of Irving and Irving (1982), this result would imply that more than 1000 km of shortening took place between South China and Eurasia, following the acquisition of the remanence. However, there is no geological evidence for this large shortening. We propose that the remanence was acquired within the time corresponding to the tip of the hairpin turn (~150-50 Ma) in the revised APWP of Besse and Courtillot (this issue). The local geology suggests that the syncline from which the samples were taken has been rotated by  $15^\circ\pm 5^\circ$  counterclockwise, which is reflected in a similar discrepancy between the measured paleodeclination and that predicted by the Besse and Courtillot (this issue) Eurasian APWP. After correcting for this rotation, the pole position is 70.9°N, 225.2°E ( $dp=2.4^\circ$ ,  $dm=6.5^\circ$ ). We conclude that Eurasia was fully assembled by the end of the Jurassic and that the Mesozoic Eurasian hairpin turn is a real feature.

## INTRODUCTION

China and Southeast Asia are recognized to form a mosaic of blocks which were accreted onto the Siberian craton during the Phanerozoic [e.g., Zhang *et al.*, 1984]. The main blocks, North China, Tarim, South China, and Indochina have Precambrian basements and contain stable sedimentary basins with paleontological records which show that these blocks had independent faunal histories, at least during the Cambro-Ordovician [e.g., Burrett, 1974]. They are often bordered by linear fold belts and fault zones, sometimes featuring ophiolites, flysch wedges, narrow zones of high-grade metamorphism and other indicators of sutures.

Accretion events are dated by paleontological study of syn-collisional sediments or geochronometry of collisionally reset or intruded rocks. Unfortunately, the foldbelts of China have often been reactivated, so the timing of these suture events is hotly debated. For example, Mattauer *et al.* [1985] date the North China - South China collision at the Devonian, while Sengör

[1984] puts it in the late Jurassic. Laveine *et al.* [1987] point out that there are notable paleontological similarities between the North and South China blocks going back to at least the lower Carboniferous. Wang [1985] notes that Permian and Triassic flora in the two blocks are quite different but do have similarities, so he suggests that North and South China collided temporarily. The timing of the Siberia - North China collision is similarly disputed. Burrett [1974] places it in the upper Permian while Sengör [1984] argues for the Jurassic-Cretaceous boundary. The most recent event was the collision of India with Eurasia, which substantially rearranged the mosaic [Molnar and Tapponnier, 1975; Tapponnier *et al.*, 1986] to its present configuration (Figure 1).

Paleomagnetism offers an independent possibility to constrain the geological history of Southeast Asia. Whereas geological evidence usually comes from the borders of the cratons, paleomagnetic investigations tend to focus on the stable interiors. Clearly, geodynamic interpretation of paleomagnetic data demands very well-determined apparent polar wander paths (APWPs). Besse [1986] and Besse and Courtillot [this issue] have reconsidered the corpus of published paleomagnetic data to propose reliable reference APWPs covering the last 200 Ma for some of the major continental blocks. The large number of studies available today allows high acceptance standards. Poles were included only if they were (1) well-defined paleomagnetically, (2) proven to be primary using field tests, (3) dated to within 15 Ma, and (4) from

<sup>1</sup>Now at Department of Geology and Geophysics, University of Edinburgh.

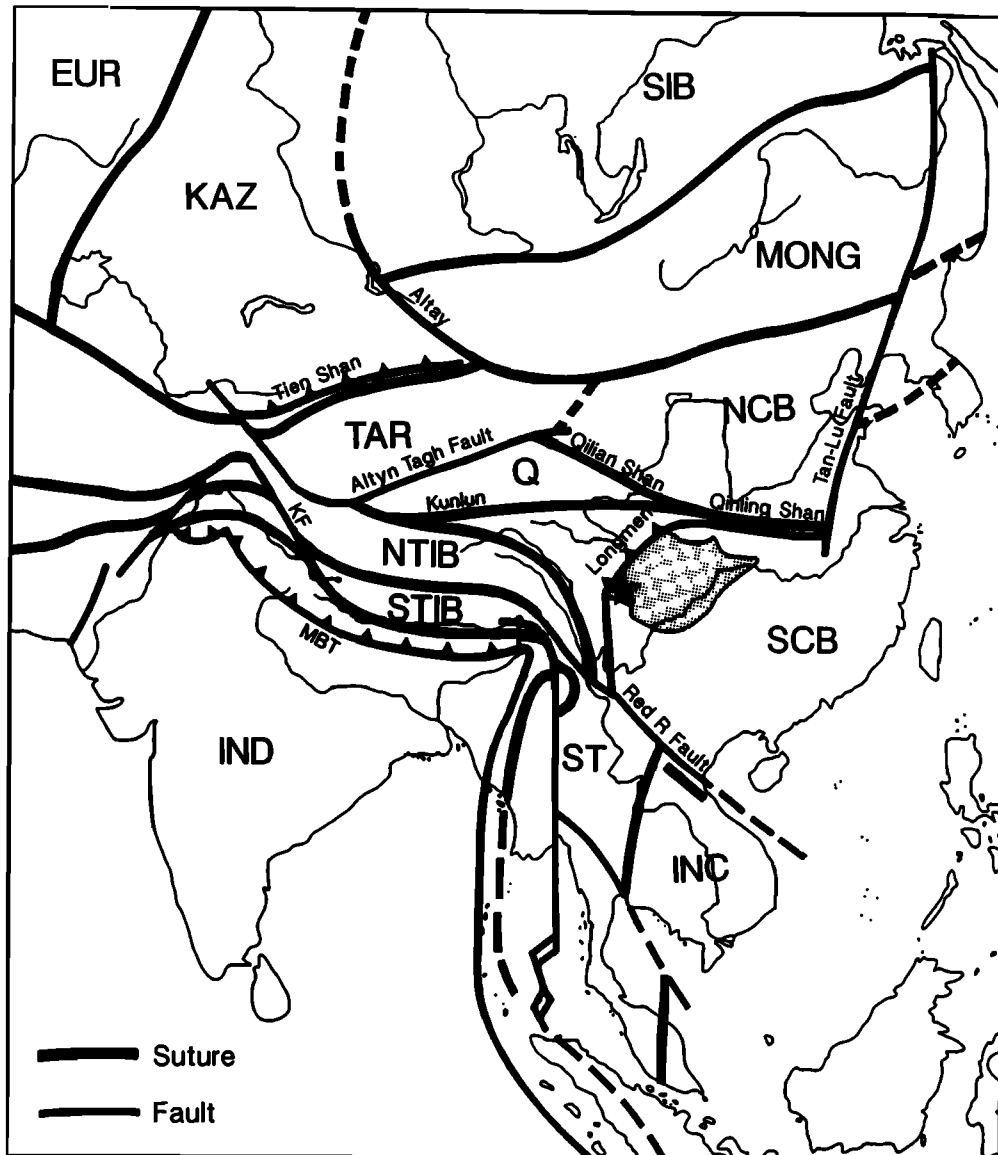


Fig. 1. Schematic tectonic map of China, showing sutures and major faults. The major blocks are EUR, Europe; KAZ, Kazakhstan; SIB, Siberia; MONG, Mongolia; TAR, Tarim; NCB, North China Block; SCB, South China Block; Q, Qaidam; NTIB, North Tibet (Qiangtang Block); STIB, South Tibet (Lhasa Block); ST, Shan Thai; INC, Indochina; and IND, India. The Sichuan Basin is the stippled region and the sampling area is marked with a star. Based on Li et al. [1982] and P. Tapponnier (personal communication, 1989).

stable cratonic regions. In total, only 101 poles from Africa, North America, Eurasia and India were admissible under these criteria. Oceanic magnetic anomalies were used to tie together the relative motions of these blocks so that all the paleomagnetic data could be pooled together. Average poles were defined using a 20-Ma moving window. The differences between the APWPs of individual blocks and this "master" APWP are not significant except that the uncertainty of the latter is much smaller ( $5^\circ$  on average).

A distinctive feature which is seen in the new Eurasian APWP is a large ( $30^\circ$ ) hairpin turn during the Mesozoic. Previous compilations [e.g., Irving and Irving, 1982] seem to have missed this significant feature, masked by the inclusion of questionable data and excessively large averaging windows. Westphal et al. [1986] and Lee et al. [1987] had noted its existence in the transferred data from other blocks.

Eurasia, because of its great extent, is a testing ground for paleomagnetic study of the rigidity of continental plates over geologic time. Lower Cretaceous poles included in the Besse and Courtillot pole list from Korea, North and South China are consistent with poles transferred from other cratons fitted with the western border of Eurasia, indicating that the entire length of the craton was rigid at that time (to within paleomagnetic uncertainties), but more data are required.

The Indian collision greatly affected Eurasia. The extrusion model of Tapponnier et al. [1986] predicts significant rotation of the Indochina (Sundaland) block which has been paleomagnetically confirmed [e.g., Chen and Courtillot, 1989]. On the other hand, the South China block should have suffered a much smaller rotation, which could be constrained with paleomagnetic data.

The number of paleomagnetic studies in China increased rapidly

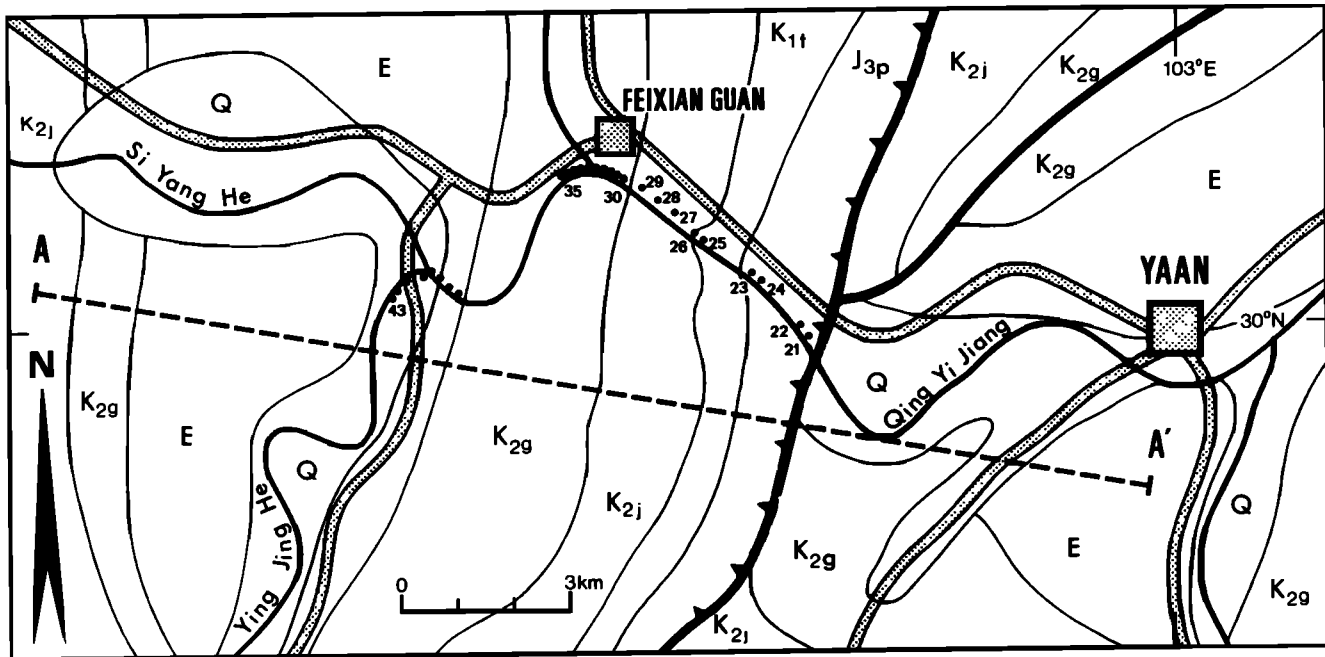


Fig. 2. Geological map of the Feixianguan section, including site locations (numbered circles). The cross section line (A-A') is shown in Figure 4. Formation names are given in Figure 3. Stippled lines are roads, medium lines are rivers and wide lines are faults. After Geological Map of Sichuan, 1:1,000,000.

in the 1980s. Due to widespread remagnetization events in China [e.g., Kent *et al.*, 1987; Zhao, 1987], it is essential to perform careful field tests and demagnetization work, and thus the earlier studies often cannot be considered reliable.

McElhinny *et al.* [1981] reported the first results using modern techniques, with their study of Permo-Triassic poles from North and South China. Their conclusions that both blocks had similar equatorial paleolatitudes but very different paleodeclinations, and that both were far south of the Siberian block at that time, have been supported by subsequent studies [Chan *et al.*, 1984; Lin *et al.*, 1985; Opdyke *et al.*, 1986; Zhao and Coe, 1987, 1989; Steiner *et al.*, 1989]. McFadden *et al.* [1988] and Li *et al.* [1988b] find that the Tarim block had an intermediate paleolatitude during the Permian. Accordingly, the paleomagnetic data prove that China was not assembled until at least the end of the Palaeozoic.

Jurassic and Cretaceous poles reported by Lin *et al.* [1985], Kent *et al.* [1986], Lee *et al.* [1987], Li *et al.* [1988a] and Chen *et al.* [1991] are concordant, apparently indicating that China was fully assembled by the end of the Jurassic. Courtillot and Besse [1986] observe, furthermore, that the middle Jurassic to upper Cretaceous poles show little directional variation with time. These poles are concordant with the standstill at the tip of the J-K hairpin turn for the Eurasian APWP as defined by Besse and Courtillot [this issue]. The body of reliable data from China is small, so more work must be done to make these conclusions firm.

A French-Chinese collaboration was organized to study the paleomagnetic record of the South China block. A clear target for paleomagnetic study is the Sichuan Basin, a large, weakly deformed red bed basin of Mesozoic age, situated in the west of the South China craton (see Figure 1). The goals of the project were (1) to place constraints on the accretion of South China onto the Eurasian craton, (2) to add data to the APWP of Eurasia, and (3) to study the deformation following the Indian collision against Eurasia. This paper presents results from the first field season (November 1986).

#### GEOLOGICAL SETTING

The Sichuan Basin, 1000 km E-W, 500 km N-S, is one of the largest red bed basins in the world. On a Sinian (Upper Proterozoic) basement, sedimentation started during the early Palaeozoic in a marine environment (the "Upper Yangtze Evaporite Sea," Wang [1985]). The seas receded during the "Early Indosinian Movement" (Middle Triassic) to form the "Chuan-Dian Basin," in which continental red beds were deposited from then on until the early Cenozoic. Geophysical studies indicate that up to 12 km of sediments fill the basin [Sun and Wu, 1984].

During our first field season we sampled in the region around the city of Ya'an (30°N, 103°E, 130 km SW of Chengdu), in the extreme west tip of the basin. Note that nine sites from a study of Otofujii *et al.* [1990] also come from this area. The exposure there is excellent, although the proximity to the Longmen Shan thrust fault system may have led to local rotations and remagnetizations. In this paper we present results from a river section (fig.2) west of Ya'an around the village of Feixianguan (completely unrelated to the Lower Triassic "Feixianguan" formation found elsewhere in the Sichuan Basin).

The section consists of a suite of massive continental red beds. Channelling at all scales up to tens of meters and numerous conglomerate layers show that the region was close to an eroding mountain chain during deposition.

The series is almost completely azoic. No fossils were found in our collection of red beds. According to the Chinese cartography, the sites were distributed in age from the Upper Jurassic to the Eocene (Figure 2). These ages are based on a very few continental ostracods (less than 100 individuals, 18 species, Li Yuwen, personal communication, 1988, see Figure 3). Most constraining in age is the species *Cypridea*, found in the lower part of the series, which existed in Europe from the Upper Jurassic (Bajocian) to the Lower Cretaceous (Albian) [Moore, 1961]. Near the top of the series are found the species *Cyprinotus*, *Eucypris*, and *Lineo-*

Level (m)	Formation	Site	Fossils
800	E2l	43	
	Lu Shan	42	
1000	E2y	41	Cyprinotus sp., Limnocythere, Lineocypris sp.
	Yu Guang Po	40	
1200	E1-K2j		
1400	Jin Gi Guan	39	
		38	
		37	Eucypris sp., Condonia sp., Nonian Sichuanensis N. Subrusticam, N. Quodatum, Condonia sp.
1600		36	Cypridia (pseudocypridina) sp., Cyprinotus sp. Honoeucypris sp., Limnocythere sp., Metacypris
1800			
2000	K2g2		Candoniella, ?Bairdia sp., Limnocythere sp.
	Upper Guan Kou		?Paracypris sp., Kosmogyras sp.
2200			
2400			
	K2g1	35a,b	
		34a,b,c	
2600	Lower Guan Kou	33a,b,c	
		31,32	
		30	
2800			
		29	?Cypridea sp.
3000			
	K1j		
3200	Jia Guan	28	
		27	
3400			?Cypridea sp.
		26	
		25	Cypridea sp., Mongoniella sp. Jingguella (Minheela) Lashanensis sp. nov.
3600			
	K1t		
3800	Tian Ma Shan		Darwinula sp.
		21,23,24	
		22	
4000	J3p		
	Peng Lai Zhen		

Fig. 3. Stratigraphic log of Feixianguan section. The zero reference level is taken at the center of the syncline. The formations and fossils are from an unpublished Ministry of Geology document.

*cypris* which lived from the Upper Cretaceous or Tertiary to the present. Continental ostracods have smooth shells with few distinctive marks, so that misidentification is not impossible. Moreover, correlations of these fossils with geological time is unsure. It is interesting (but somewhat disturbing) to note that formation boundaries usually occur at massive conglomerate beds.

The 3 km of sediments show a cyclic deposition, going from conglomerates to fine-grained sandstones. There are no lithological trends in the series; the facies, color and texture remain consistent throughout. There are no visible unconformities.

The Feixianguan section has a rather simple cylindrical structure shown in Figure 4. Most sites were on one limb of a 20-km syncline bound on the west by the Longmen Shan Thrust. The syncline thrusts eastward over a neighboring syncline, producing

a small anticlinal drag fold with steep dips, providing two sites suitable for a fold test. The stratigraphic levels of the sites sampled on the drag fold are difficult to define with the available data, but they correspond roughly to the bottom of the monoclinical series.

#### FIELDWORK

Sites ZS21 to ZS43 were collected along this section. Preliminary work [Zhuang *et al.*, 1988] suggested that the river section behind the village of Feixianguan included the end of the Cretaceous Long Normal Superchron (CLNS). Accordingly, this stretch was sampled at higher density in an attempt to establish a magnetostratigraphic correlation. We divided the 168 samples of the magnetostratigraphic sites (ZS30 - ZS35) into 11 sites (each of about 25 m stratigraphic thickness) for the purpose of calculating the global magnetic direction average. Thus a total of 28 sites were taken.

Standard 2.5-cm-diameter cores were taken with an electric drill, with lengths varying from 3 to 12 cm depending on rock hardness. Usually 12 or 14 cores were drilled per site, distributed over many meters of stratigraphic thickness and taken with varying azimuths to avoid systematic sampling errors. Cores were oriented with a magnetic compass. Solar azimuths were rarely taken, due to the dominantly overcast weather. Differences between the 51 solar and magnetic azimuths are normally distributed around  $0.7^{\circ}W \pm 1.0^{\circ}$ , slightly different from the  $1.4^{\circ}E$  declination of the 1986.8 International Geomagnetic Reference Field. A magnetic declination of  $0.7^{\circ}W$  was used for all magnetically determined azimuths and bedding strikes.

All sites have uniform bedding (except ZS24 and ZS41 which were slightly folded or faulted), the bedding attitude being determined as an average of 3 to 15 independent measurements. The bedding orientations of neighboring sites which were clearly parallel were averaged. The main source of bias may possibly have arisen from not having recognized very large scale channel structures.

#### LABORATORY INVESTIGATION

Samples from each site were measured by both laboratories; odd numbered samples were measured in the Academy of Geology Paleomagnetism Laboratory in Beijing, and even numbered samples in the Institut de Physique du Globe de Paris. A total of 450 specimens (2.2 cm long) from 373 cores were measured.

Most specimens were thermally demagnetized, in both cities in laboratory-built furnaces. Remanence was measured with a Schönstedt DSM-2 fluxgate magnetometer in Beijing, and with a CTF 3-axis SQUID magnetometer in Paris. Twenty specimens were demagnetized in Paris with a Schönstedt alternating field (AF) demagnetizer. This interlaboratory comparison was extended

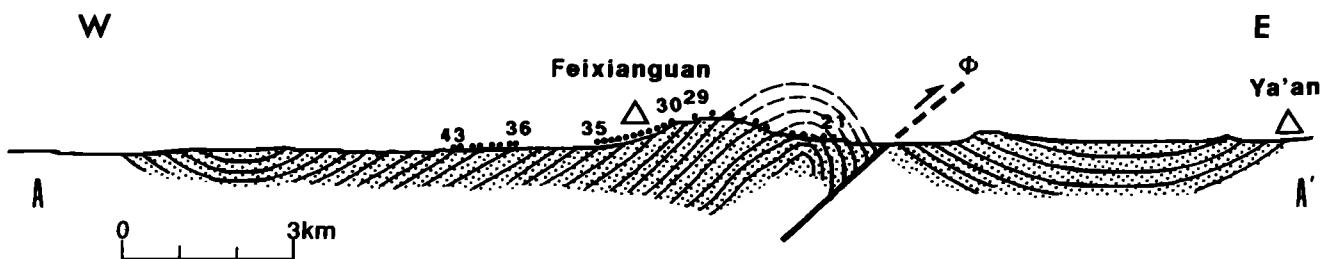


Fig. 4. Cross section of the Feixianguan section (location given in Figure 2). Only one limb of the syncline was sampled, but drag on the fault (marked  $\phi$ ) folded this otherwise monoclinical limb, allowing a fold test. The frontal thrusts of the Longmen Shan are about 10 km west of this section (compare Figure 18).

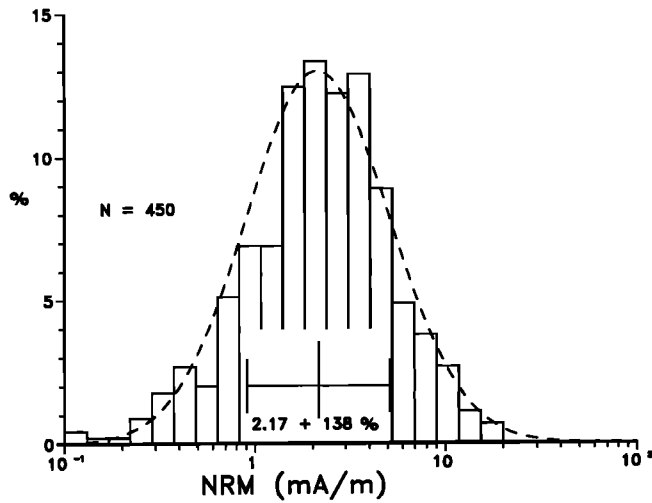


Fig. 5. Logarithmic histogram of NRM intensity. The collection follows a lognormal distribution marked with the dashed curve.

to the Department of Earth Sciences, Oxford University, England, where 18 specimens were demagnetized (Magnetic Measurements furnace, CCL SQUID magnetometer) and to the Centre des Faibles Radioactivités, at Gif-sur-Yvette, France (10 specimens, Pyrox furnace, LETI SQUID magnetometer).

The samples were usually demagnetized over 10 to 18 steps, the sample orientation in the furnace being changed at each step to detect systematic parasitic remagnetization.

After each step of one run of 60 specimens measured in the Paris laboratory, the bulk susceptibility of each specimen was measured using a Minisep susceptibility bridge, and its color was compared to the Munsell color system, to monitor chemical changes [e.g., *Holm and Verosub*, 1988].

Paleomagnetic directions and planes were calculated using principal component analysis [*Kirschvink*, 1980]. Site means were calculated using McFadden's method [*McFadden and McElhinny*, 1988], which reduces to the traditional Fisher average when directions alone (and not remagnetization planes) are averaged. To estimate the mean direction of a combination of sample directions

TABLE 1. Site Data

Site	Level m	Form'n	S,D	Specim mA/m	NRM	+/-	$K_N$ °C	MDT °C	$T_B$
21	3850	J3p	44,77	10/12	3.86	80%	0.4	650	650
22	3950	J3	44,77	10/19	4.50	61%	0.9	600	650
23	3850	J3p	200,26	15/19	0.476	84%	0.3	300	remag
24	3875	J3p	188,25	18/22	2.83	54%	0.6	500	650
25	3525	K1t	219,35	4/13	0.570	123%	0.1	???	remag
26	3450	K1t	219,35	12/14	0.848	93%	0.5	600	650
27	3350	K1t	192,38	12/18	1.00	56%	0.2	350	remag
28	3200	K1j	203,26	7/13	2.92	116%	0.6	600	650
29	2950	K1j	207,25	13/13	10.66	53%	1.4	650	680
30	2750	K1j	192,30	13/14	6.68	54%	1.0	600	680
31	2675	K2g1	190,26	11/12	1.27	51%	-	200	remag
32	2650	K2g1	190,26	17/19	1.35	41%	-	450	650
33A	2625	K2g1	190,25	18/18	1.19	99%	-	400	650
33B	2600	K2g1	190,25	23/25	3.06	77%	-	400	680
33C	2575	K2g1	190,25	19/19	2.38	49%	-	500	680
34A	2550	K2g1	188,23	19/20	2.71	51%	-	550	680
34B	2525	K2g1	188,23	20/20	3.16	24%	-	400	680
34C	2500	K2g1	188,23	11/13	2.72	26%	-	250	650
35A	2475	K2g1	189,26	19/20	2.96	58%	-	300	680
35B	2450	K2g1	189,26	17/17	3.30	59%	-	400	680
36	1575	K2g2	189,26	11/13	1.56	138%	0.2	400	650
37	1550	K2g2	189,25	12/14	1.71	43%	0.1	200	remag
38	1400	E1j	195,22	13/13	1.20	65%	0.1	250	remag
39	1300	E1j	194,23	14/16	1.64	125%	0.2	200	remag
40	1100	E2y	185,27	8/13	2.23	147%	0.2	200	600
41	1025	E2y	189,27	17/17	1.81	174%	0.2	350	650
42	925	E2l	196,22	9/11	4.95	67%	1.4	550	680
43	850	E2l	196,22	13/13	3.28	37%	0.6	600	680

Site number (with magnetostratigraphic site 33 to 35 divided for equal weighting in the average), stratigraphic level where the zero reference level is taken at the center of the syncline, formation code (full names given in Figure 3), strike (S) and dip (D), number of specimens used in average / number of specimens measured, average NRM intensity, spread (+/-) one logarithmic standard deviation, Koenigsberger ratio ( $K_N$ ), average mean destructive temperature (MDT), and average unblocking temperature ( $T_B$ ).

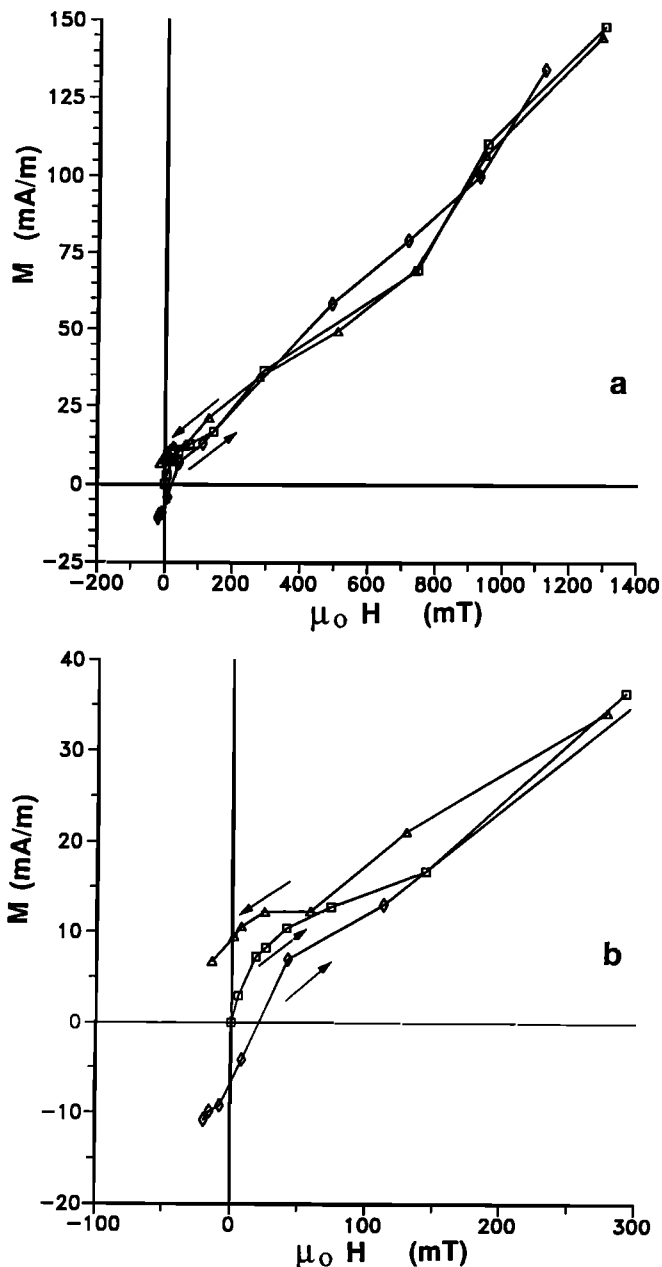


Fig. 6. Translating sample magnetometer magnetization curve for sample ZS38-10A. The curve for large negative  $H$  was not measured, but the sample was magnetized in  $-1.3$  T before measuring the bottom branch. (a) Full curve, (b) enlargement of the central 300-mT interval to show the hysteresis loop of the soft component.

and great circles (with or without sector constraints), the method consists of iteratively finding the direction such that the Fisher average of the sample directions and the points on the great circles closest to this direction results in this same direction. These closest points are estimates of the final directions hidden in the noise. The uncertainty estimate comes from a modification of the Fisher precision parameter. The inclusion of sector constraints on the great circles reduces the problem of bias in the determination of the intersection.

#### ROCK MAGNETISM

The natural remanent magnetization (NRM) intensities have a lognormal distribution (Figure 5) with geometric mean of 2.17

$\text{mA/m} \pm 138\%$ , where the spread is  $1\sigma$ . The within-site scatter (Table 1) is quite small (average  $\pm 75\%$ ), and there is a negative correlation between the magnetization intensity and magnitude of the site level  $\alpha_{95}$ .

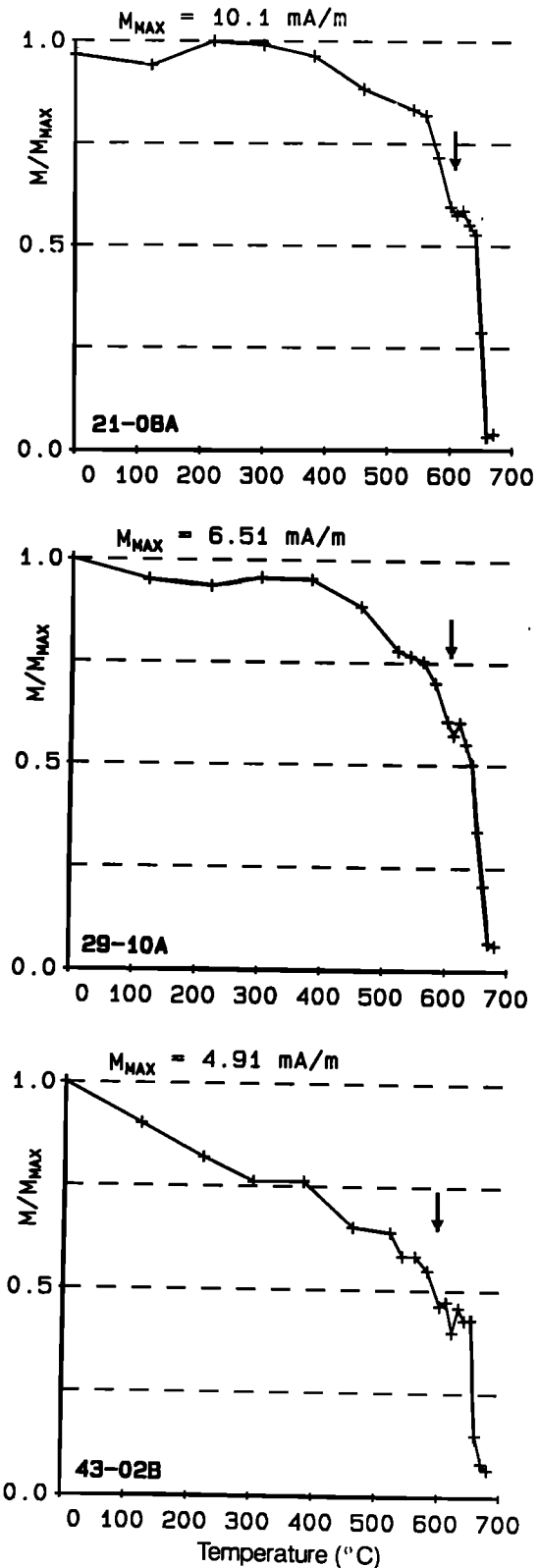


Fig. 7. Normalized demagnetization intensity curves for samples which clearly show a drop at  $580^{\circ}\text{C}$  (marked with arrows), indicating the presence of magnetite. Almost all samples had an intensity drop at  $660^{\circ}\text{C}$ , expected from hematite in red beds.

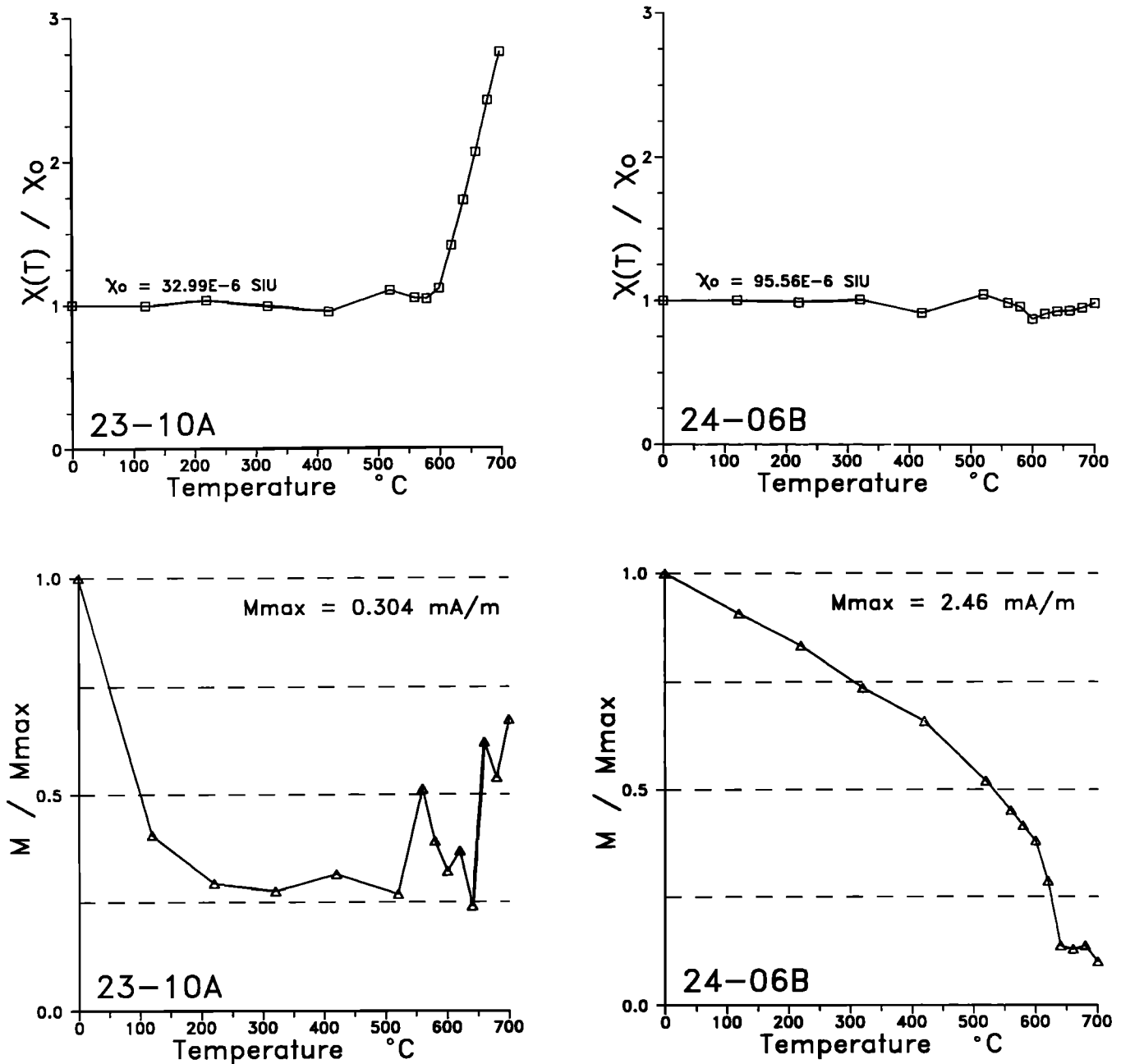


Fig. 8. Susceptibility and intensity curves for representative specimens from sites ZS23 and ZS24. All samples from ZS23 showed unstable susceptibility and incoherent magnetic directions after high temperature steps, while ZS24 samples were well behaved to the final demagnetization steps.

The Koenigsberger ratio ( $K_N = M_{\text{NRM}} / \chi_0 H_0$ ,  $\mu_0 H_0 = 50 \mu\text{T}$ ), with a roughly lognormal distribution (geometric mean =  $0.31 \pm 132\%$  ( $1\sigma$ )), is quite low for single-domain pigmentary hematite. In igneous rocks,  $K_N$  below 0.5 indicates a dominance of multidomain grains, but magnetization acquisition of red bed hematite is a chemical or sedimentary rather than thermal process. So either this low value of  $K_N$  is caused by poorly magnetized single-domain hematite grains, or there is a non-negligible multidomain component. We now show, using other rock magnetic indicators, that there is indeed a multidomain component present in these rocks.

Magnetization curves were measured for five samples with the translating sample magnetometer (TSM) of the Geomagnetic

Observatory in St. Maur, France. Each curve has a hysteresis loop of relatively low coercivity between 20 and 40 mT. By 100 to 400 mT, this internal loop saturates and from there to the peak field of 1.3 T, the curves rise linearly (Figure 6). This final linear segment cannot be just the paramagnetic susceptibility of the rock mass because the AF demagnetization of the NRM was never complete up to 100 mT (i.e., well above the coercivity measured on the TSM). Less than 30% of the NRM was demagnetized by 20 mT each time, above which the magnetic vector remained relatively stable. The low coercivity component shown in the TSM measurements and AF demagnetizations is independent of the hard hematite component.

The magnetic viscosity of the collection is not high, despite the

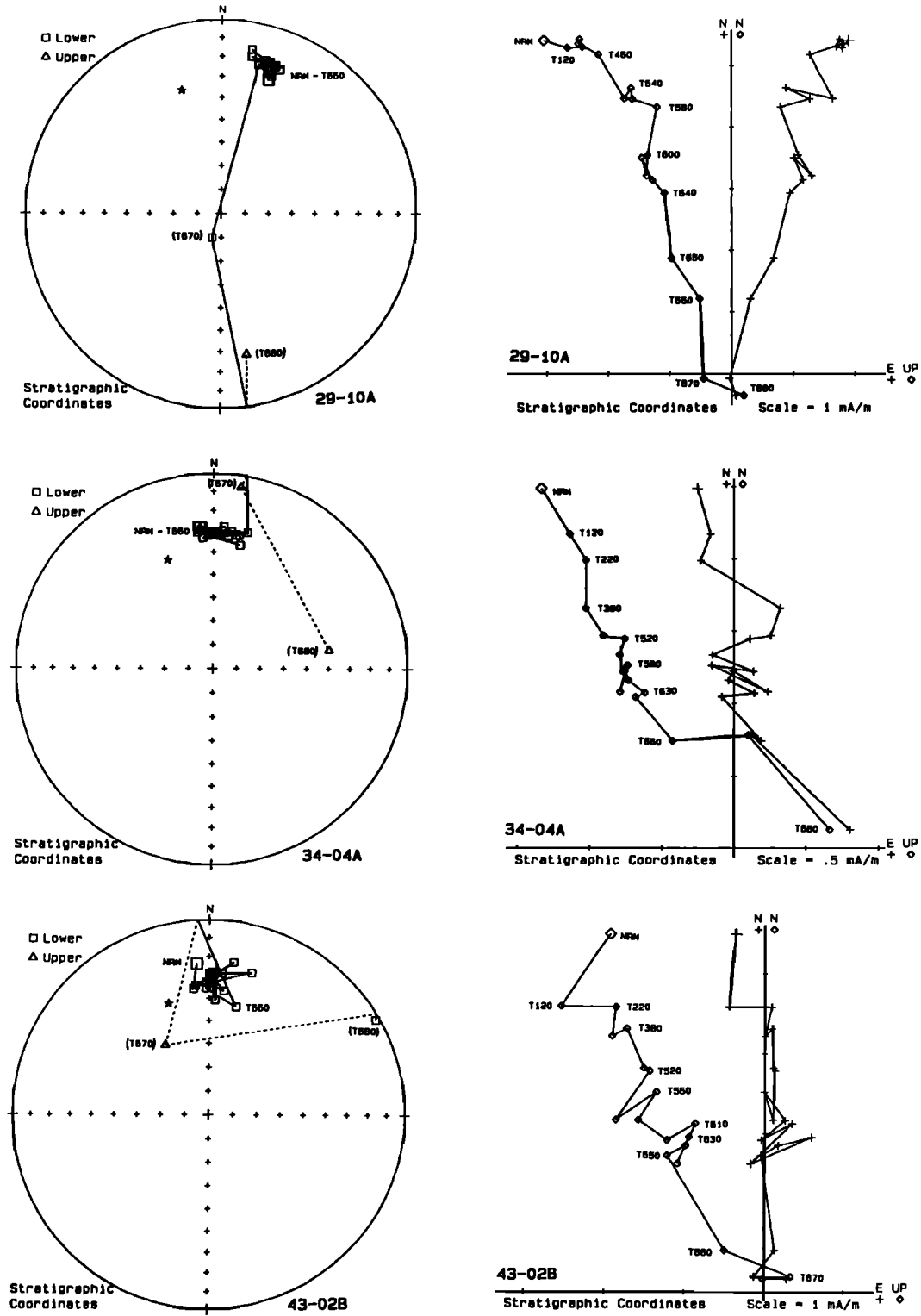


Fig. 9. Representative stereographic and vector Zijderveld diagrams (in stratigraphic coordinates) of specimen demagnetizations. Demagnetization temperatures given in degrees Celsius, present Earth field (after structural correction) marked with a star.

low coercivity magnetic carriers. When a demagnetization run was interrupted for a week or even for months, the remanence was usually remeasured before the following demagnetization. The intensity of the subtracted vector divided by the NRM intensity had a roughly lognormal distribution ( $N=256$ ) with mean  $3.1 \times 10^{-2}$  and a spread of 128% around the mean ( $1\sigma$ ). The difference measured is a combination of the in-lab viscous remanent mag-

netization and the measuring noise, so in fact the viscosity may even be smaller than this measure indicates.

Sometimes there is a large decrease in the magnetization after thermal demagnetization of the NRM to about 580°C, the Curie temperature of magnetite, before a final unblocking above 660°, related to hematite (Figure 7). The maximum unblocking temperature of NRM ( $T_{ub}$ ) averaged over each site (Table 1) was almost

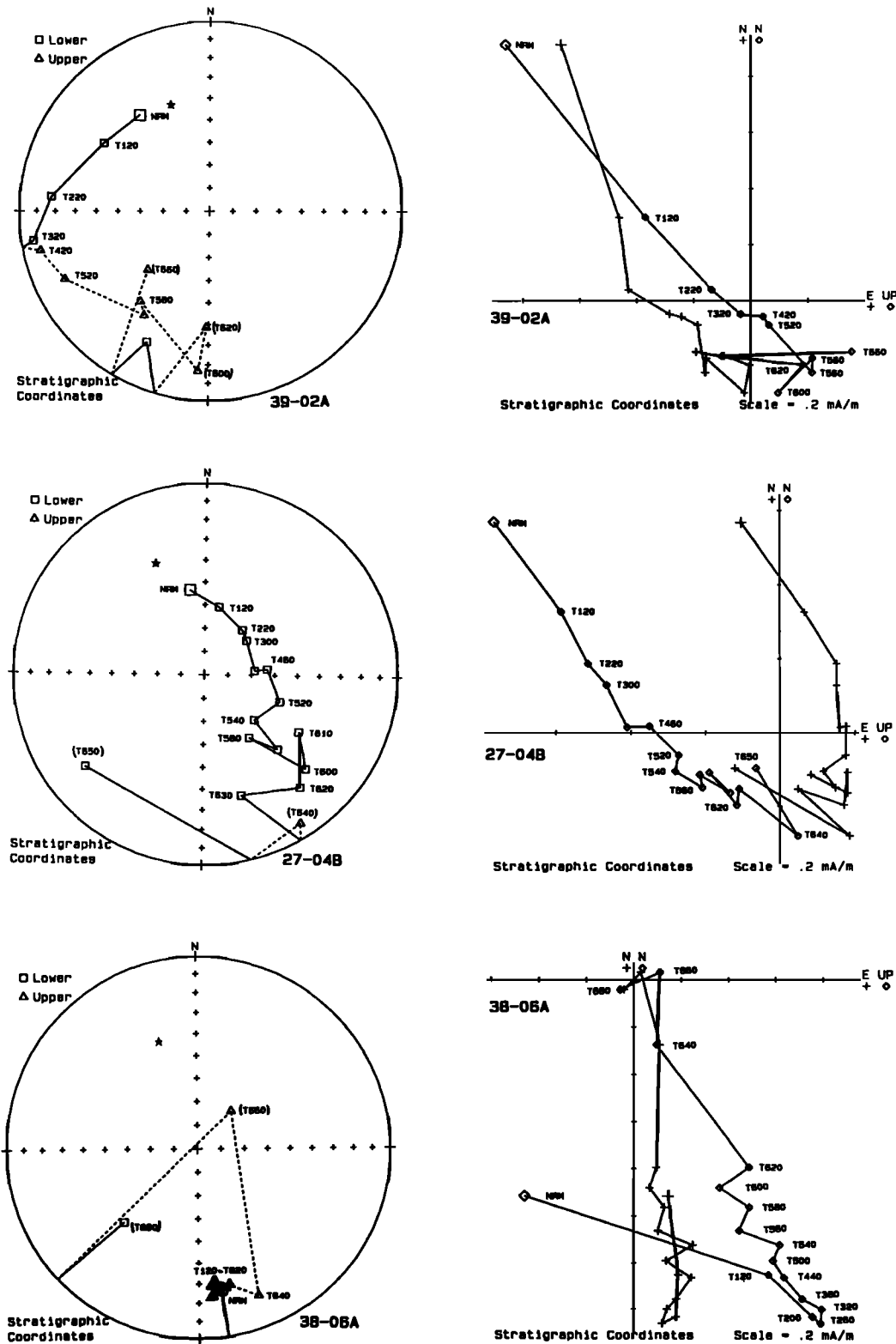


Fig. 9. (continued)

always above 600°C, showing that hematite is present. The mean destructive temperature (MDT) was variable throughout the study, but within-site dispersion was small enough to allow site averages to be estimated (table 1). Three quarters of the sites have MDTs under 600°C, indicating that the soft component is dominant. Most often, primary directions were stable from well under 580°C up to the Curie temperature of hematite, which implies that both

soft (magnetite or large grained hematite) and hard (pigmentary hematite) carriers were magnetized in the same direction. This constitutes a stability test in those samples which contain magnetite, because red pigmentary hematite forms during diagenetic chemical alteration, whereas magnetite quite possibly carries an original depositional remanence.

The susceptibility of well-behaved samples (i.e., those which

demagnetized linearly toward the origin) was relatively constant after all temperature steps. Samples with erratic remanent directions after high temperature demagnetization steps tended to have large increases in susceptibility at the same steps (Figure 8). With this proof of the growth of new magnetic carriers in the furnace, we are justified in not looking for paleomagnetic information in the final steps of these samples. We also tried to monitor color changes, but while we could see a qualitative reddening in most samples, the matching of specimens to Munsell color chips showed no recognizable trends.

#### RESULTS

*Zijderveld* [1967] and stereographic diagrams of representative samples from the collection are given in Figure 9. Thermal demagnetization of nearly every sample from the Feixianguan traverse revealed two paleomagnetic components, often separable (e.g., ZS29-10A). The two components usually overlapped in reversely magnetized samples, but a great circle (with sector constraints) could almost always be determined (e.g., ZS27-04B, ZS39-02A). Rarely, a reverse direction could be isolated from a specimen (e.g., ZS38-06A)

The low temperature component (LTC) was usually demagnetized by 400°C. The LTC direction (defined along the first

linear component of the demagnetization diagram) was highly scattered (Figure 10), with a circular standard deviation (CSD) of 25.9° about the mean ( $D=1.0^\circ$ ,  $I=49.7^\circ$ ,  $k=9.8$ ,  $\alpha_{95}=2.5^\circ$ ,  $N=350$ ), which is clearly the present Earth field (PEF) direction ( $I=49^\circ$ ). Not all 450 specimens are included because sometimes no LTC component could be isolated. The precision factor  $k$  is 1.7 times larger in geographic than in stratigraphic coordinates, which gives a highly significant negative fold test, considering the size of the sample. A curious and incoherent inverse overprint was seen in the samples from one site (ZS34) measured in Beijing, while the high temperature direction was the same from the two laboratories.

Even in sites which have very well-behaved high temperature components (HTCs), the LTCs can be quite scattered. The HTC of site ZS43, for example, has a CSD of only 7.2°, while the LTC is distributed with a CSD of 18.1°. Perhaps a random post-sampling viscous remanence is superimposed on the PEF direction, but this is difficult to explain considering the low in-laboratory viscosity.

AF demagnetization was never complete, and the component removed was roughly in the PEF direction (geographic coordinates:  $D=358.6^\circ$ ,  $I=37.2^\circ$ ,  $k=9.0$ ,  $\alpha_{95}=23.7^\circ$ ,  $N=6$ ). This average direction gives a negative fold test ( $k_2/k_3 = 2.4$ ) showing that this component is postfolding. When the remaining component was in

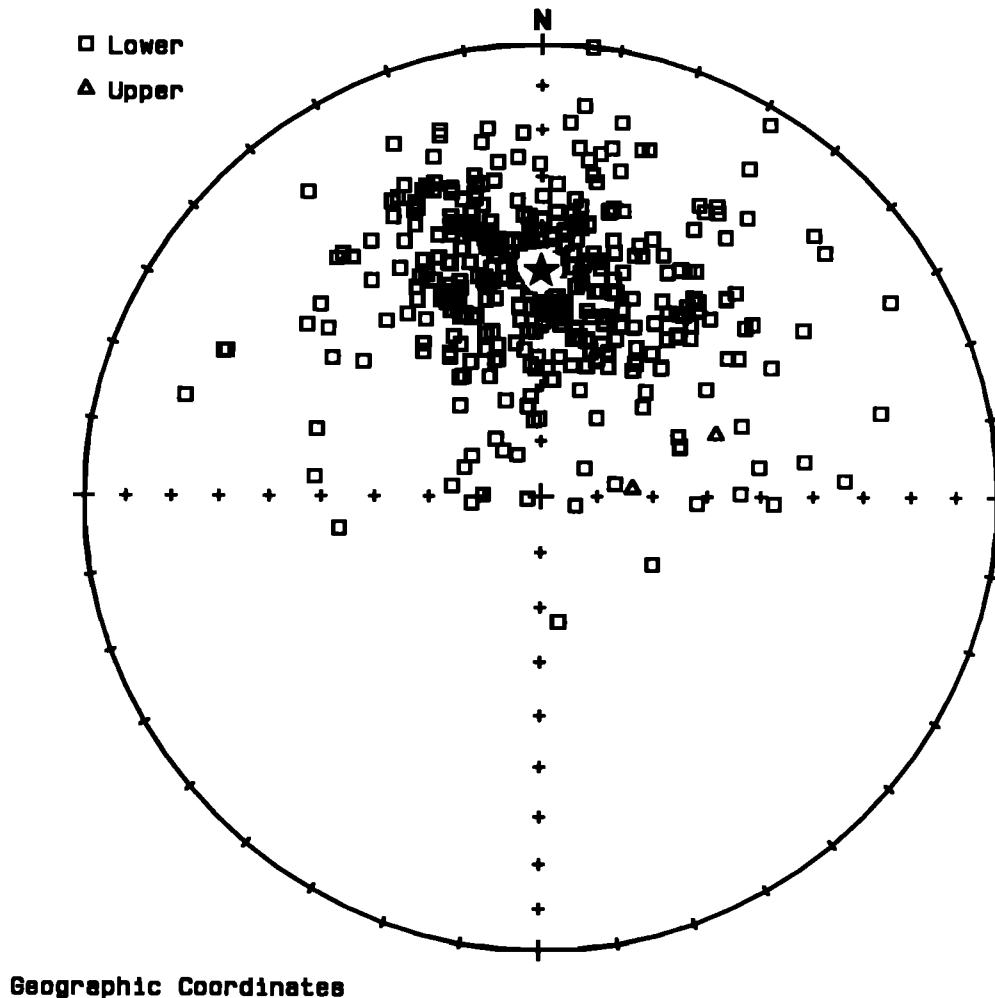


Fig. 10. Stereographic projection of the low temperature component of 350 specimens in geographic coordinates. The mean (star) coincides with the present Earth field.

a direction coherent with the thermally treated specimens from the same site, it was included in the site average.

When determining a direction by principal component analysis (PCA), it is important to decide whether to force the lines through the origin. The problem is particularly important in the case of red beds, which can acquire a subsequent chemical remanent magnetization with higher blocking temperature than the "primary" magnetization. An equivalent problem is posed in the case of determining planes: if there is a hidden component which does not demagnetize, then a small circle must be calculated instead of a great circle. One could argue that the origin should never be forced, because a line to the origin will naturally intersect it. This argument does not take into account the increased impact of noise when the origin is not forced. The final demagnetization steps, which are most prone to noise, can "anchor" a PCA line in the wrong direction if the origin is not forced.

In the present study the HTC's at some sites were clearly directed to the origin; that is, deviations around the best fitting straight line were greater than the line's deviation from the origin (e.g., Figure 9, ZS29-10A, ZS43-02B). Unfortunately, other sites were affected by chemical changes during high temperature steps (as shown by changes in susceptibility), and the final stages of demagnetization towards the origin were masked (e.g., Figure 9, ZS34-04A). In these cases, it was impossible to be sure if a

higher unblocking temperature component was hiding in the "true" final approach to the origin. It must be emphasized however that no sites in the Feixianguan section gave any systematic indication of a hidden unresolvable overprint.

We tested the method of forcing the directions to the origin by doing PCA with and without the origin forced on the samples from sites 22 and 30, two sites in which demagnetization never reaches the origin but for which linear segments could still be fit. For both sites, the  $\alpha_{95}$  dropped slightly (but insignificantly) when the origin was forced, from 11.0° to 10.0° for site 22, and from 11.2° to 10.9° for site 30. Note that the site average directions changed by 3.9° and 3.4° respectively, not statistically significant given the size of the  $\alpha_{95}$  but enough to affect the site-level average. A few samples clearly contained a component which missed the origin, and no attempt was made to force these demagnetization lines to pass through it. Because these samples were anomalous with respect to the normal behavior in the collection, we generally rejected the corresponding data from the site-level averages.

McFadden averages were calculated for the sites (Table 2), rejecting only extremely inconsistent specimens (most often with no recognizable linear segments). Despite the noisy nature of the demagnetizations, only 14% of specimens were rejected. When both polarities are present in a site, the directions were inverted to the dominant polarity and averaged together. In general, averages

TABLE 2. Site Directions

Site	Specim	Normal	D <sub>0</sub>	I <sub>0</sub>	D <sub>s</sub>	I <sub>s</sub>	k	$\alpha_{95}$	$\lambda$	$\pm$
21	10/12	100%	355.3	-16.5	9.3	39.9	19.7	11.3	22.7	8.2
22	10/19	100%	0.9	-7.3	23.4	39.6	26.8	9.5	22.5	6.8
23	15/19	0%	185.3	-36.5	170.3	-26.4	12.9	11.5	13.9	6.8
24	G S	18/22	100%	19.1	43.3		31.8	6.2		
					355.2	42.4	25.2	7.0	24.5	5.3
25	4/13	0%?	194.8	-28.1	183.7	-10.2	5.5	50.8	5.1	26.0
26	12/14	100%	32.1	50.4	0.3	36.0	41.8	6.8	20.0	4.6
27	12/18	0%	203.9	-28.7	182.0	-29.3	12.4	13.4	15.7	8.2
28	7/13	100%	45.2	41.2	20.3	45.7	12.1	18.1	27.1	14.7
29	13/13	100%	39.6	26.7	26.3	28.7	38.8	6.7	15.3	4.1
30	13/14	100%	23.0	22.8	9.0	24.6	15.7	10.8	12.9	6.2
31	11/12	0%	185.6	-50.2	159.0	-41.8	26.0	10.0	24.1	7.5
32	17/19	0%	196.5	-34.2	178.7	-33.1	40.5	5.9	18.1	3.8
33A		18/18	0%	189.9	-35.0	173.9	-31.1	28.3	6.9	16.8.3
33B		23/25	100%	29.9	32.8	11.9	37.3	28.2	5.8	20.0.0
33C		19/19	84%	22.6	37.8	2.4	38.6	21.0	7.1	21.8.0
34A		19/20	100%	22.6	27.4	9.8	30.9	44.3	5.1	16.3.2
34B		20/20	100%	19.2	32.7	3.9	34.3	72.9	3.9	18.8.6
34C		11/13	100%	17.3	34.6	1.1	35.2	19.0	10.9	19.7.3
35A		19/20	68%	18.5	31.8	2.1	32.4	30.6	6.2	17.4.0
35B		17/17	100%	18.6	27.3	4.5	28.5	53.5	5.1	15.3.1
36	11/13	64%	15.0	35.9	356.5	34.3	28.2	8.9	18.8	5.8
37	12/14	25%	186.5	-35.8	170.0	-30.8	30.0	8.7	16.6	8.7
38	13/13	0%	190.1	-33.1	177.3	-28.7	23.7	9.0	15.3	5.4
39	14/16	0%	188.5	-33.0	175.3	-28.0	32.2	7.6	14.9	4.6
40	8/13	0%	190.6	-32.8	173.3	-30.9	47.8	9.4	16.7	5.9
41	G S	17/17	35%	200.1	-39.5		39.9	7.9		
					176.2	-40.2	57.1	4.9	22.9	3.6
42	9/11	100%	334.4	21.3	330.5	6.0	145.6	4.3	3.0	2.2
43	13/13	100%	17.0	32.5	3.5	30.2	125.9	3.7	16.2	2.3

Site number, number of specimens used in average / number measured, proportion of normal polarity samples, declination and inclination in geographic and stratigraphic coordinates, Fisher distribution parameters k and  $\alpha_{95}$ , paleolatitude  $\lambda \pm$ uncertainty dp.

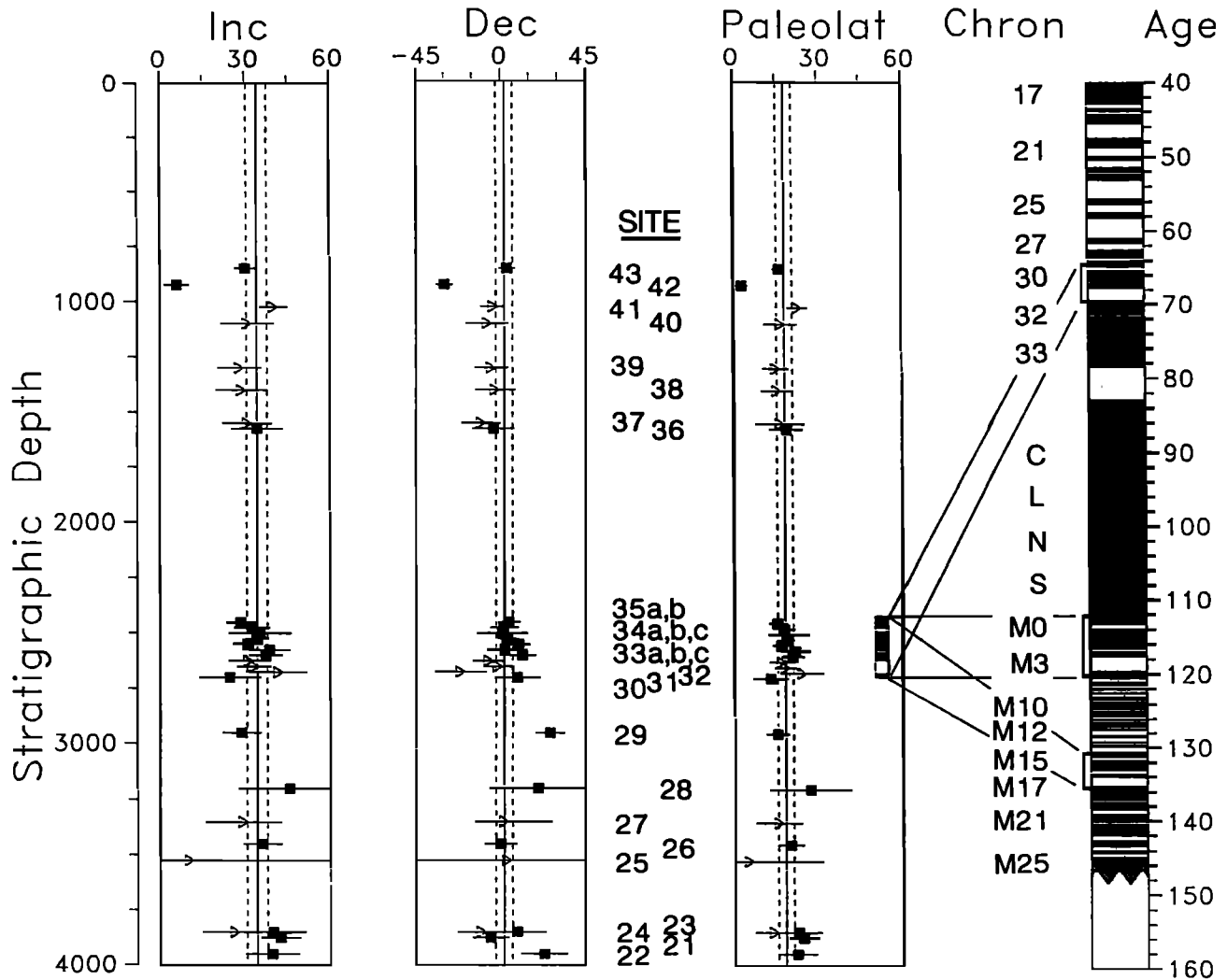


Fig. 11. Stratigraphic column of site mean directions. Normal polarities are represented with solid squares, the antipodes of reversed polarities are given with open triangles. The solid (respectively dashed) lines correspond to the overall means (with 95% significance uncertainties) for inclination, declination and paleolatitude. The slopes of the best fitting lines are never significantly different from zero, indicating that the paleofield did not change during the timespan of magnetization acquisition. The polarity time scale is positioned such that it correlates sites ZS30 to ZS35b with chron M4 to the bottom of the Cretaceous Long Normal Superchron (compare fig. 16), and two other possible (but rejected) correlations are shown. The M series is from Lowrie and Ogg [1986], while the upper series is from Cox [1982].

for reversely magnetized sites had to be determined by intersection of great circles.

The paleomagnetic direction hardly varies over the entire stratigraphic column (Figure 11). A least squares linear fit of the inclination versus stratigraphic level (stratigraphic coordinates, excluding ZS25 and ZS42) gives a variation of  $1.8 \pm 2.4^\circ/\text{km}$  over the 3 km thickness (the uncertainty gives the 95% confidence interval); the declination varies by  $3.9 \pm 4.5^\circ/\text{km}$ , and the paleolatitude varies by  $1.2 \pm 1.6^\circ/\text{km}$ . These "trends" are not significantly different from zero. Accordingly, we hypothesize that all the sites can be taken together for a global average.

The site means are plotted in Figure 12, and it is clear that the directions are well grouped in both polarities. The colatitude plot [Fisher *et al.*, 1987] (Figure 13) shows that the dispersion of directions is well modeled by the Fisher distribution, except for six outliers which warrant discussion.

Site ZS25 was weakly magnetized and very easily chemically altered in the furnace. Few specimens showed any signal above the noise. With an  $\alpha_{95}$  of  $50.8^\circ$ , this site is statistically indistin-

guishable from the rest, but its average direction was not included in the global average. Site ZS28 had similar though far less severe problems ( $\alpha_{95}=18.1^\circ$ ) which we considered small enough to save the site in the average.

Site ZS22 is one of the two sites on the east limb of the fold, so for the fold test it is critical that the characteristic direction of this site be isolated. While site ZS21 was well behaved, samples from ZS22 often had a pronounced contamination by the PEF. By rejecting all specimens in which the PEF direction amounted to more than about 25%, the average moved  $11.2^\circ$  from the PEF toward the global average direction (Figure 12). Nevertheless, the ZS22 direction sits somewhat outside the mass, in the direction of the PEF (after structural correction), and we can assume that the overprint was not completely eliminated.

Site ZS31 has reverse polarity, and the great circles of demagnetization are mostly subparallel. The great circles mark the path from the PEF to the final direction, and if these two end points have no dispersion, one would expect all samples to demagnetize along exactly the same path. An unconstrained intersection defines

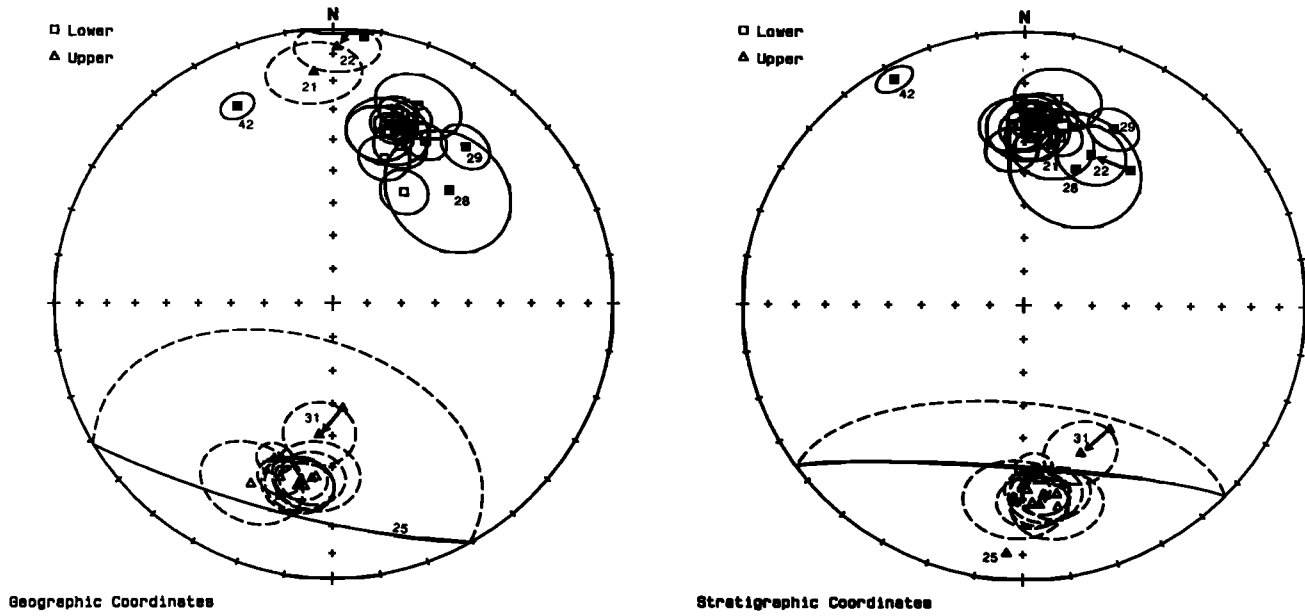


Fig. 12. Stereographic projections of site means with their  $\alpha_{95}$  circles of uncertainty: (left) geographic coordinates, with a star marking the present Earth field; (right) stratigraphic coordinates. The outlying site directions discussed in the text are marked with solid symbols. The curve pointing to ZS22 originates at this site's average when all specimens are included. The arrow pointing to ZS31 originates at this site's intersection when sector constraints are not taken into account (compare fig. 14).

a direction midway between one endpoint and the antipode of the other, thus introducing a "bias" in the determination of the final direction [McFadden and McElhinny, 1988]. The effect of sector constraints in the McFadden average in this site is shown in Figure 14. The average moves  $10.2^\circ$  toward the global average with the inclusion of constraints. One can assume that there remains a bias

even with sector constraints. (Note that the intersection is not significantly different from the antipode of the PEF.)

The most remote outlier, site ZS42, is the most difficult to explain. The direction is very well defined, with an  $\alpha_{95}$  of only  $3.2^\circ$ . The site was taken from a riverside outcrop, continuous with site ZS43, from which it is separated by only 50 m. The same

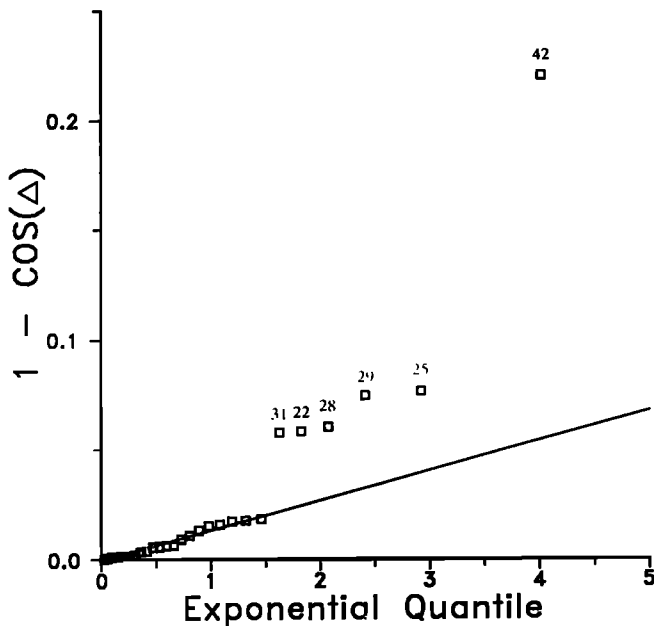


Fig. 13. Colatitude plot [Fisher et al., 1987] of site means.  $\Delta$  is the angular distance (colatitude) of the site mean with respect to the global mean. The abscissa increases logarithmically after the sites were sorted in order of increasing  $\Delta$ . If the points follow a Fisher distribution, the points should lie on a line through the origin. The sites that do not fit the Fisher distribution are identified and discussed in the text.

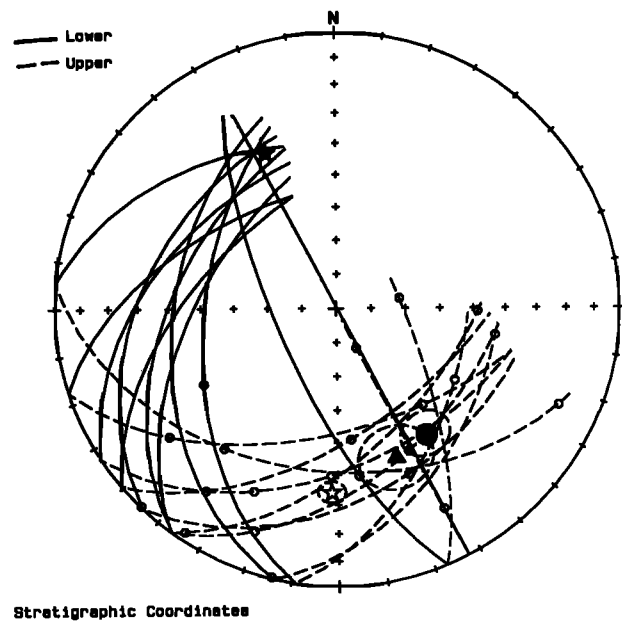


Fig. 14. Present Earth field bias of ZS31 great circle intersection. Each great circle is the best fitting plane for one specimen, marking demagnetization from the PEF to the hidden underlying component. The solid circle shows the best estimate mean when sector constraints are not taken into account. The sector constraints, marked by the small open circles on each path, help pull the site mean (triangle) away from the antipode of the PEF (solid star) toward the global mean (open star).

structural correction was used for the two sites. The rocks from these two sites look identical and have similar NRM intensities (so it is unlikely that one was remagnetized by lightning). The LTC is nearly identical in the two sites (ZS42:  $D=349.2^\circ$ ,  $I=33.3^\circ$ ,  $k=17.7$ ,  $\alpha_{95}=14.8^\circ$ ,  $N=7$ ; ZS43:  $D=349.7^\circ$ ,  $I=39.6^\circ$ ,  $k=20.0$ ,  $\alpha_{95}=9.9^\circ$ ,  $N=12$ ). There can be no laboratory error; the cores had a range of sampling orientations and sites were not demagnetized together. Both the Beijing and Paris labs obtained identical results. The virtual geomagnetic pole (VGP) of the site is not close to the APWP of Eurasia for any age, so it not a straightforward overprint. The average direction of all sites does not significantly change with the inclusion of this site (Table 3), but it is clearly not a member of the ensemble and we are forced to reject it as an as yet unexplained anomaly. Magnetostratigraphic sampling of the entire exposure would have to be carried out to solve the puzzle. Site ZS29 is another well-behaved site with a direction rather far from the mean ( $21.4^\circ$ ), but we accepted it for the global mean.

To summarize, the site means conform to a Fisher distribution for 22 of the 28 sites. The directions of the six outlying sites are dispersed around the mean because they have been affected by independent processes and thus do not produce a systematic error. We feel that only site ZS25 with a large  $\alpha_{95}$ , and ZS42 with a clearly anomalous direction should be rejected. The site level Fisher average directions for various combinations of sites are summarized in Table 3. In order to see the progression of the average with depth, we split the series into three groups, divided by the sites ZS30 to ZS35B (sampled at high magnetostratigraphic density). The first group, ZS21 to ZS29 is the oldest, and the third group, ZS36 to ZS43 is the youngest, lying above a 1-km lacuna over the second group (Figures 2 to 4).

The site mean remanence directions pass both the *McElhinny*

[1964] and the *McFadden and Jones* [1981] fold tests at the 99% level. The *McElhinny* fold test statistic  $k_s/k_G$  is 2.7 for all sites, well above the threshold for significance: 1.5 at the 95% level, and 1.8 at the 99% level. Assuming that the period of deposition is so long that the west limb only corresponds in age with the first few east limb sites, we do the test for the bottom group of sites, ZS21 to ZS29:  $k_s/k_G$  is 4.8, much greater than the thresholds for  $N=8$  (2.5 at 95%, 3.7 at 99%).

The structural corrections of the west limb sites are not all the same (Figure 15). The tilt correction improves the clustering of the sites from the west limb ( $k_s/k_G=1.15$ ), but not significantly. We can also check the specimen means from the two nonuniformly tilted sites (Table 2). In site ZS24,  $k_s$  is worse than  $k_G$  by a factor of 0.8, while better in site ZS41 by a factor of 1.4. In neither case is the test significant. (Note also that due to the erosional state of ZS24, the dips could not be accurately defined, so the structural corrections may be questionable.)

While the *McFadden and Jones* [1981] fold test appears to be more pertinent to the present study, a strict application is not possible due to the variation in bedding on the west limb. It is a test of whether the directions of two limbs are statistically distinguishable, but the statistic depends on the distributions rather than the directions themselves. In theory, one is comparing the distribution, described by the parameter  $R$  (the length of the resultant vector), for each limb in geographic coordinates to the distribution of the whole in stratigraphic coordinates, or vice versa. But when a limb has a nonuniform structure, the distribution is modified on correction so the resultant  $R$  changes between the two coordinate systems and the comparison cannot be made. If the bedding planes within each limb are similar it is appropriate to calculate the  $R$  variables in the same coordinate system.

The value  $(R_E+R_W-R_T^2/(R_E+R_W))/2(N-R_E-R_W)$ , where subscripts E,

TABLE 3. Fisher Average of Site Groupings

Collection	N		Geographic Coordinates				Stratigraphic Coordinates								
	n		D	k	$\alpha_{95}$	D	k	$\alpha_{95}$	I	$k_s/k_G$	$\lambda$	Lat.	Long.		
All	26	372	17.1	32.0	23.0	6.0		2.0	34.2	63.1	3.6	2.7	18.8	78.6	273.4
All (with ZS42)	27	381	15.4	31.9	19.9	6.4		0.7	33.4	41.4	4.4	2.1	18.2	78.2	279.7
Normal	16	235	20.3	29.3	16.4	9.4		7.4	35.2	76.3	4.3	4.7	19.4	77.5	248.9
Reverse	10	137	191.9	-36.0	109.9	4.6		173.8	-32.2	125.2	4.3	1.1	17.5	76.3	308.7
ZS21 - ZS29	8	97	18.8	27.0	7.9	21.1		8.1	36.7	38.1	9.1	4.8	20.4	78.0	243.7
ZS30 - ZS35B	11	187	18.8	33.4	87.2	4.9		1.8	33.7	86.2	4.9	1.0	18.4	78.3	274.5
ZS36 - ZS43	7	97	12.5	34.7	290.0	3.6		356.0	31.9	219.3	4.1	0.8	17.3	76.8	299.9
ZS21 - ZS29 NOR	6	70	20.2	24.7	5.9	30.1		12.7	39.3	48.7	9.7	8.3	22.3	76.2	224.2
ZS21 - ZS29 REV	2	27	195.0	-32.9	-	-		176.1	-28.0	-	-	-	14.9	74.5	297.2
ZS30 - ZS35B NOR	8	132	20.9	30.8	183.4	4.1		5.4	32.5	183.4	4.1	1.0	17.7	76.7	260.0
ZS30 - ZS35B REV	5	55	198.5	-38.4	53.8	10.5		178.5	-37.6	50.0	10.9	0.9	21.1	81.0	291.9
ZS36 - ZS43 NOR	4	29	22.4	32.6	41.7	14.4		5.2	34.3	37.8	15.1	0.9	18.8	77.9	258.9
ZS36 - ZS43 REV	6	59	192.3	-34.8	242.7	4.3		175.4	-32.2	222.7	4.5	0.9	17.5	77.3	294.3
Paris	26	228	16.6	32.8	20.3	6.5		1.1	34.8	55.5	3.8	2.7	19.2	79.1	277.5
Beijing	26	144	19.2	28.4	20.6	6.4		6.0	31.9	36.6	4.8	1.8	17.3	76.2	258.3
West Limb	24	352	19.0	35.2	59.9	3.9		0.9	33.7	68.9	3.6	1.2	18.4	78.4	278.7
West Limb, ZS21-ZS29	6	77	27.5	38.6	30.9	12.2		5.5	35.5	32.6	11.9	1.1	19.6	78.5	256.1
East Limb	2	20	358.1	-11.9	-	-		16.4	40.0	-	-	-	22.8	73.6	215.4

N sites, containing n specimens, declination (D), inclination (I), precision parameter k and 95% significance angle  $\alpha_{95}$ , in geographic and stratigraphic coordinates, the ratio of precision parameters in the two coordinate systems ( $k_s/k_G$ ), paleolatitude  $\lambda$ , and VGP latitude and longitude.

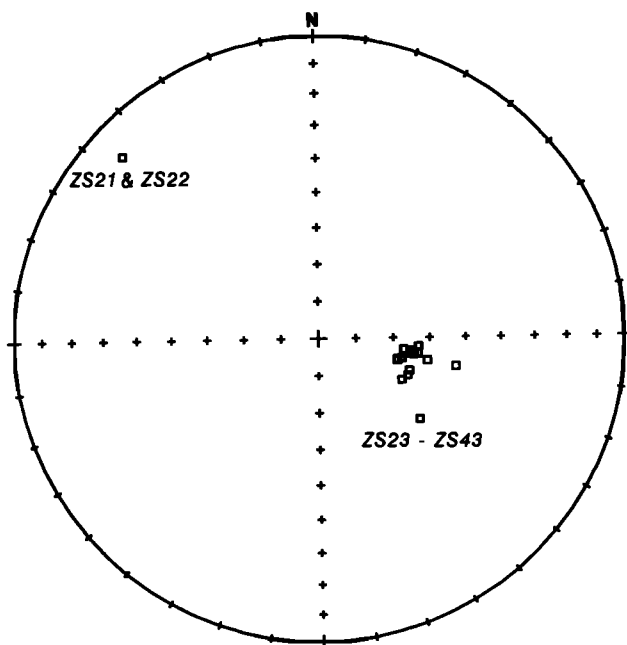


Fig. 15. Stereographic projections of the normals to the bedding planes at each site.

W and T stand for east limb, west limb and total respectively, is 1.7 for all sites in geographic coordinates (4.0 for sites ZS21 to ZS29), well above the 95% and 99% thresholds for significance, 0.13 and 0.21 (0.65 and 1.15), respectively. Therefore the hypothesis that the two limbs have a common true mean direction before structural correction is soundly rejected. On the other hand, in stratigraphic coordinates, the statistic is 0.08 (0.13 for the lower eight sites), substantially below the threshold values given above, so the two limbs do not have statistically distinguishable true mean directions. Therefore using both methods, we have a positive fold test and we can conclude that the remanence is pre-folding and stable.

The comparison between laboratories lends confidence to the results. Samples for the Paris and Beijing labs were taken side by side, so a sample by sample comparison could be done. For instance, mixed polarity sites always have the same polarity sequence. The average directions from the two laboratories taken separately do not differ significantly (Table 3).

The comparison with the few samples demagnetized in Oxford and Gif-sur-Yvette also supports the credibility of the results. We went to these laboratories because of concern that the poor quality of a number of the demagnetization paths measured in Paris might be due to our equipment. We found that sister specimens of poorly behaved specimens measured in Paris always showed similar behavior in the other laboratories. More stable samples did have similar unblocking spectra and directions which were within  $5^{\circ}$ - $10^{\circ}$  of each other. The dispersion in directions is comparable to the dispersion of sister samples which were both measured in Paris. For example, within-core HTC direction differences from site ZS24 were  $5^{\circ}$ - $18^{\circ}$  for samples measured in Paris, while specimens from ZS24-12 measured in Paris and Oxford differed by  $6^{\circ}$ .

The average directions of the two polarities taken separately are not antipodal, by  $11.9^{\circ} \pm 8.6^{\circ}$  (see Table 3). Two interpretations are suggested. It is possible that there was apparent polar wander during deposition and that we are not justified in making one global average. Because the proportion of reverse polarity sites

increases as we go up the sedimentary column (Figure 11), the mismatch could just come from averaging the field at different times. The offset is primarily in declination, which would imply a rotation during sedimentation. The other possibility is that the intersections of great circles used to find the reverse site averages are biased [McFadden and McElhinny, 1988], as discussed in the case of ZS31. The antipode of the average of the reverse sites is in fact shifted with respect to the normal sites in the direction of the PEF after bedding correction. In either case the error is small, so we interpret the reversals to be indicative of primary remanence.

Sites ZS30 to ZS35b consist of 272 m of uniform red sandstone sampled at 83 levels. The magnetic sequence is of dominantly normal polarity with a (1) relatively long reverse interval near the bottom and (2) brief reverse intervals higher up (Figure 16). Assuming a relatively constant rate of sedimentation and no missing polarity intervals, we find three plausible correlations with the Jurassic-Cretaceous geomagnetic polarity time scale (see Figure 11): (1) from chron 32.1 to 29 (69 to 64 Ma [Cox, 1982], 46.2 m/Ma); (2) chron M4 to the bottom of the CLNS (120 to 113 Ma [Lowrie and Ogg, 1986], 33.0 m/Ma); (3) chron M18n to M15n (135 to 130 Ma [Lowrie and Ogg, 1986], 51.5 m/Ma). The second possibility fits almost perfectly with the polarity time scale with no variations in sedimentation rate. The initially suspected age, just above the CLNS, correlates only if subchron 32r-1 is missing and the sedimentation rate varies from 4.6 m/Ma during chron 33 to 71.3 m/Ma during chron 32.2, which we consider unlikely.

While it is certainly dangerous to apply a linear extrapolation to determine the ages of the other sites, the CLNS provides a constraint which can be used to eliminate incorrect correlations. The first correlation, although it is the only one which is in the Upper Cretaceous and thus fits with the mapped age, would imply that reverse polarity sites ZS23, ZS25 and ZS27 were magnetized during the CLNS. Likewise, the third correlation would imply that all sites from ZS37 up should come from the CLNS, while they all contain reverse polarity samples except for the top two sites. Unlike the other two possibilities, the second correlation fits the other sites to the polarity time scale with a minor amount of stretching. The CLNS would therefore correspond to the unfortunately positioned gap in sampling between sites ZS35b and ZS36, as shown in Figure 11. This correlation is the only one which predicts that the other sites span from the Upper Jurassic to the beginning of the Tertiary, as shown by the (scant) fossil record. The correlation at this level is not perfect, however: the sites ZS36-ZS41 all contain reversed polarity samples, while the time

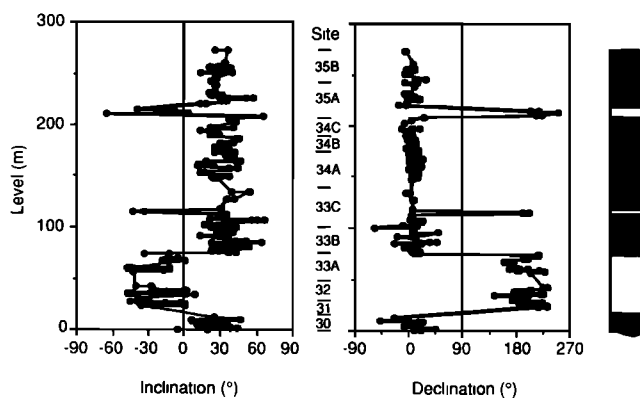


Fig. 16. Specimen directions and polarity interpretation of the magnetostratigraphic section (ZS30-ZS35b).

period in which they should fall predict dominantly normal polarity. Yet, the sampling of the reversal time scale by these sites is clearly very sparse and we feel that this problem is less significant than the problem of a series of sites contradicting the CLNS.

We conclude that the 3-km-thick Feixianguan red bed sequence records a single prefolding remanence featuring both polarities with direction  $D=2.0^\circ$ ,  $I=34.2^\circ$ ,  $k=63.1$ ,  $\alpha_{95}=3.6^\circ$ ,  $N=26$  sites (Table 3). Despite the remarkably stationary direction, it is highly unlikely that we are reporting a remagnetization since: (1) a correlatable reversal record was observed, (2) the direction passes the fold test, (3) the samples show little viscous behavior and (4) magnetite carriers seem to carry the same direction as the dominant hematite. The pole of the structurally corrected sites is at  $78.6^\circ\text{N}$ ,  $273.4^\circ\text{E}$  ( $dp=2.4^\circ$ ,  $dm=4.1^\circ$ ), corresponding to a paleolatitude of  $18.8^\circ\pm 2.4^\circ$ .

#### DISCUSSION

We compare our result with other Cretaceous poles from China in Figure 17. The first-order observation is that most poles are in agreement, despite the range in age. The present study is the first which shows, through relatively continuous sampling throughout this period, that there is no significant variation of the pole position with time (compare Figure 11). Note that *Li et al.* [1988a] perform a fold test on two series of different ages, implicitly assuming that the pole was stationary at this time.

Sichuan had the same paleolatitude as that predicted by the other Chinese poles, which we indicate in Figure 17 with the small circle centered on Ya'an going through its pole. The only pole which is not intersected by this circle and thus lay at a paleolatitude incompatible with the others is the Cretaceous-Tertiary Boundary pole from Nanjing [*Kent et al.*, 1986]. This pole might be reporting a younger age than the rest, but we note, however, that with the pole's relatively large  $A_{95}$  ( $10.3^\circ$ ) the difference is not highly significant.

The local geology suggests that the  $15^\circ$  counterclockwise (CCW) discrepancy between our pole and most of the others is the result of a local rotation. The faults and axes of the neighboring synclines, as well as the fault plane solution of a 1970 earthquake just north of the sampling region, almost all strike in a  $\sim\text{N}45^\circ\text{E}$  direction (Figure 18). The notable exceptions are the axis of the syncline we sampled and the fault which forms its eastern limit, both of which have a roughly  $\text{N}30^\circ\text{E}$  strike. The fault is mapped as terminating about 50 km north of our traverse, where it turns into an anticlinal fold. The stress field which produced the Longmen Shan fault system possibly rotated the syncline around a fixed point at the north termination of the fault through  $15^\circ\pm 5^\circ$  CCW. After removing this rotation, the pole position is  $70.9^\circ\text{N}$ ,  $225.2^\circ\text{E}$ ,  $dp=2.4^\circ$ ,  $dm=6.5^\circ$ , where  $dm$  is the Pythagorean sum of the uncertainty due to remanence dispersion and our estimate of the local rotation uncertainty.

Confirmation of this local rotation is given by Cretaceous poles

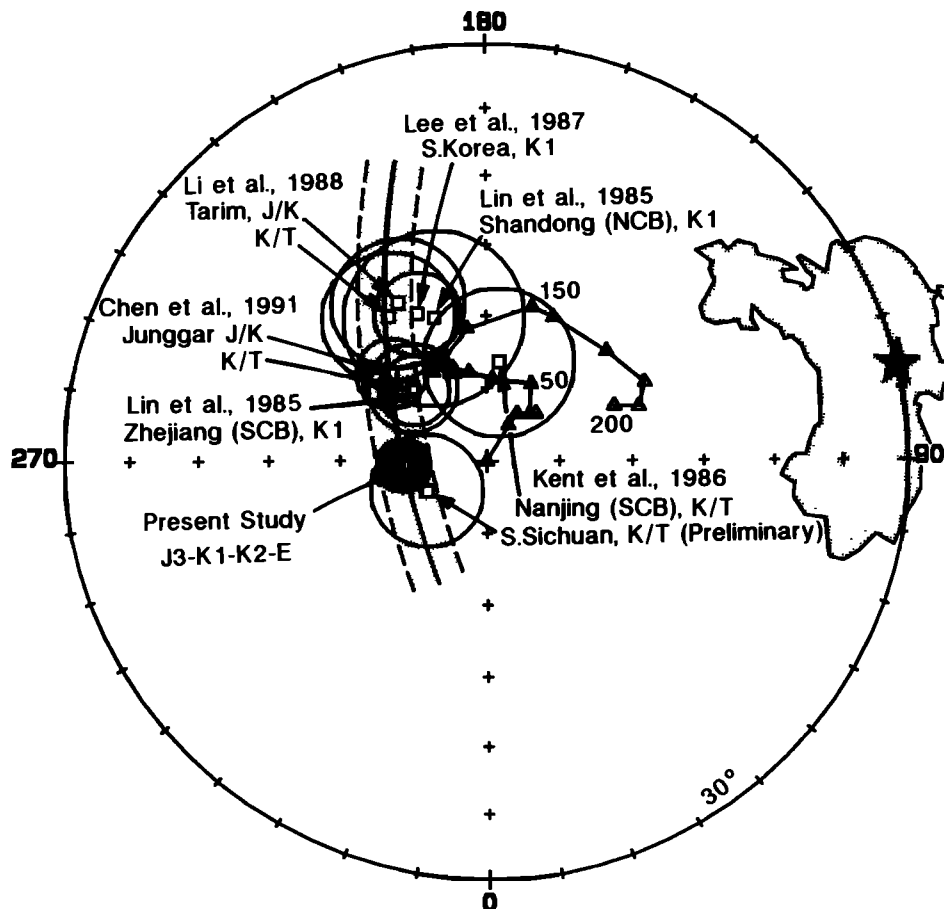


Fig. 17. Cretaceous poles from China. The small circle centered on Ya'an (star) emphasizes that all poles can be reconciled given minor tectonic rotations (see text). The Besse and Courtillot [this issue] Eurasian APWP is marked in triangles.

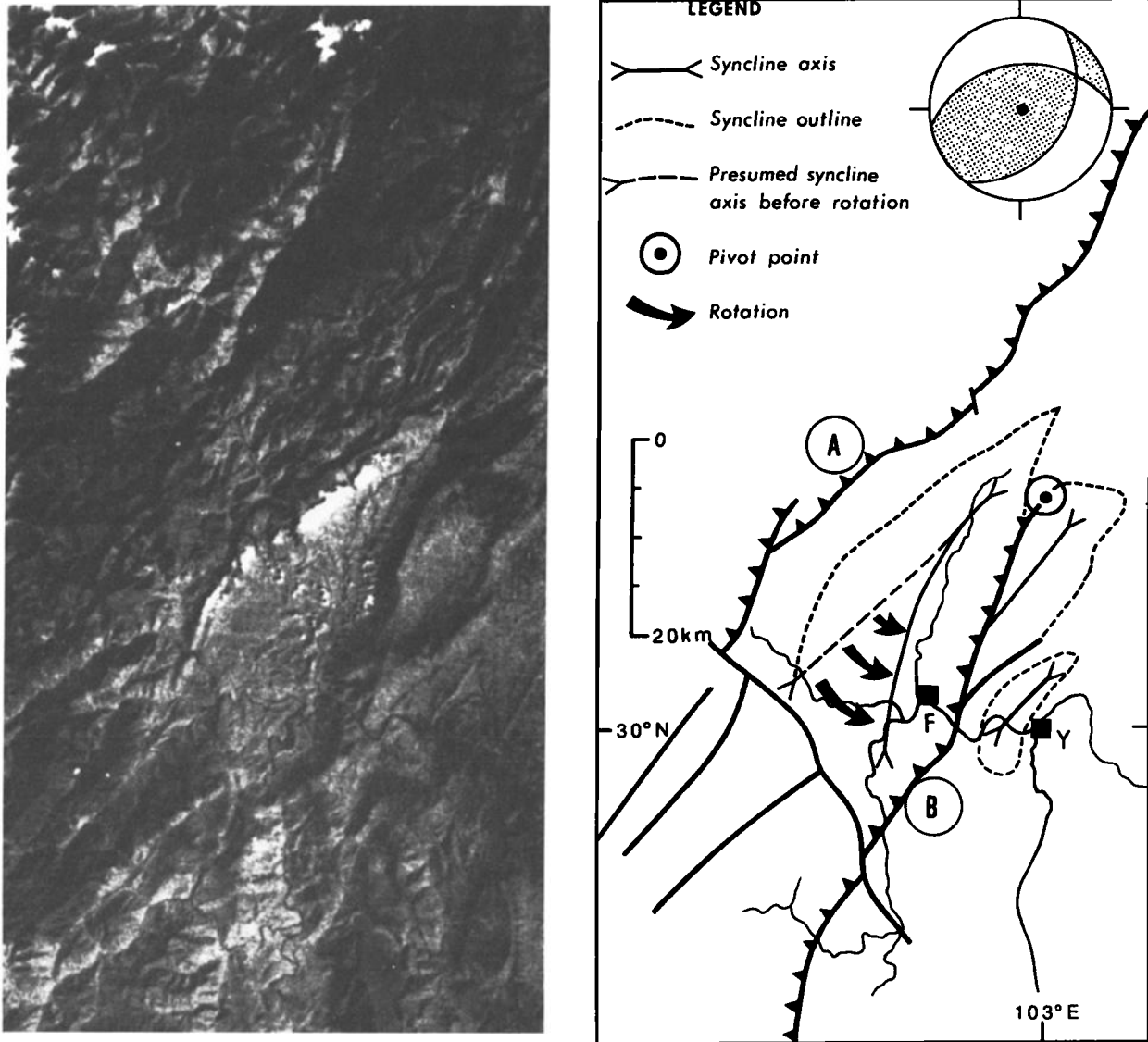


Fig. 18. (Left) Landsat photograph of the region. (Right) Sketch synopsis of this photograph, using the Geological Map of Sichuan, 1:1,000,000, showing faults (heavy lines), fault plane solution of a 1970 earthquake [Tapponnier and Molnar, 1977] and syncline fold axes (thin lines with inverted arrows). Only the frontal thrusts of the Longmen Shan (A) are marked; there are many more to the northwest. The axis of the syncline containing Feixianguan (F), and its bounding fault (B) are not parallel to the regional trend; rather they seem to have rotated about 15° CCW around a pivot point near the northeast end of fault B.

isolated from three other localities separated by up to 200 km from Feixianguan, presented in a second paper arising from the French-Chinese collaboration in the Sichuan basin [Erkin *et al.*, 1991]. The poles from Xinjin (site: 30.4°N, 103.8°E, pole: 71.0°N, 214.8°E,  $dp=8.6^\circ$ ,  $dm=14.5^\circ$ ) and Guanyin (site: 29.1°N, 104.6°E, pole: 71.7°N, 229.1°E,  $dp=5.0^\circ$ ,  $dm=8.8^\circ$ ) are coherent with each other and with the "corrected" Feixianguan pole. Note that in this latter paper, we obtain an independent measure of the rotation using a balanced section to quantify the amount of shortening due to folding and faulting, resulting in  $8^\circ \pm 5^\circ$  CCW.

Otofujii *et al.* [1991] reports a pole isolated from nine sites of three hand samples each taken from the Ya'an region, of which four (sites 76 to 79) lie in the same syncline as Feixianguan. The distribution of remanent directions from these four sites is more tightly grouped after tectonic correction ( $k_s/k_G = 2.9$ ) and give a remanent direction  $D=5.8^\circ$ ,  $I=34.0^\circ$ ,  $k=42.4$ ,  $\alpha_{95}=14.3^\circ$  which is

coherent with our result. Our analysis of the local geology predicts that his five sites located to the east of the fault bounding the Feixianguan syncline should not have suffered the 15° CCW rotation. The remanent directions from these sites are unfortunately quite highly dispersed without improvement on tectonic correction ( $D=359.3^\circ$ ,  $I=27.8^\circ$ ,  $k=14.4$ ,  $\alpha_{95}=20.9^\circ$ ,  $k_s/k_G = 1.1$ ), so no conclusion can be drawn.

Kent *et al.* [1986] present a pole (based on 12 hand samples) from south Sichuan which also seems to have suffered a  $\sim 15^\circ$  CCW rotation. There is reason to believe that the rotation in this case is on a more regional scale, because Permo-Triassic poles from the Emeishan Basalt (which has been sampled in a number of regions around the Cretaceous site [Zhao and Coe, 1987]) are generally displaced about 10° CCW from the well defined Permo-Triassic poles from the Sichuan Basin [Steiner *et al.*, 1989].

To summarize, our pole is coherent in paleolatitude with the

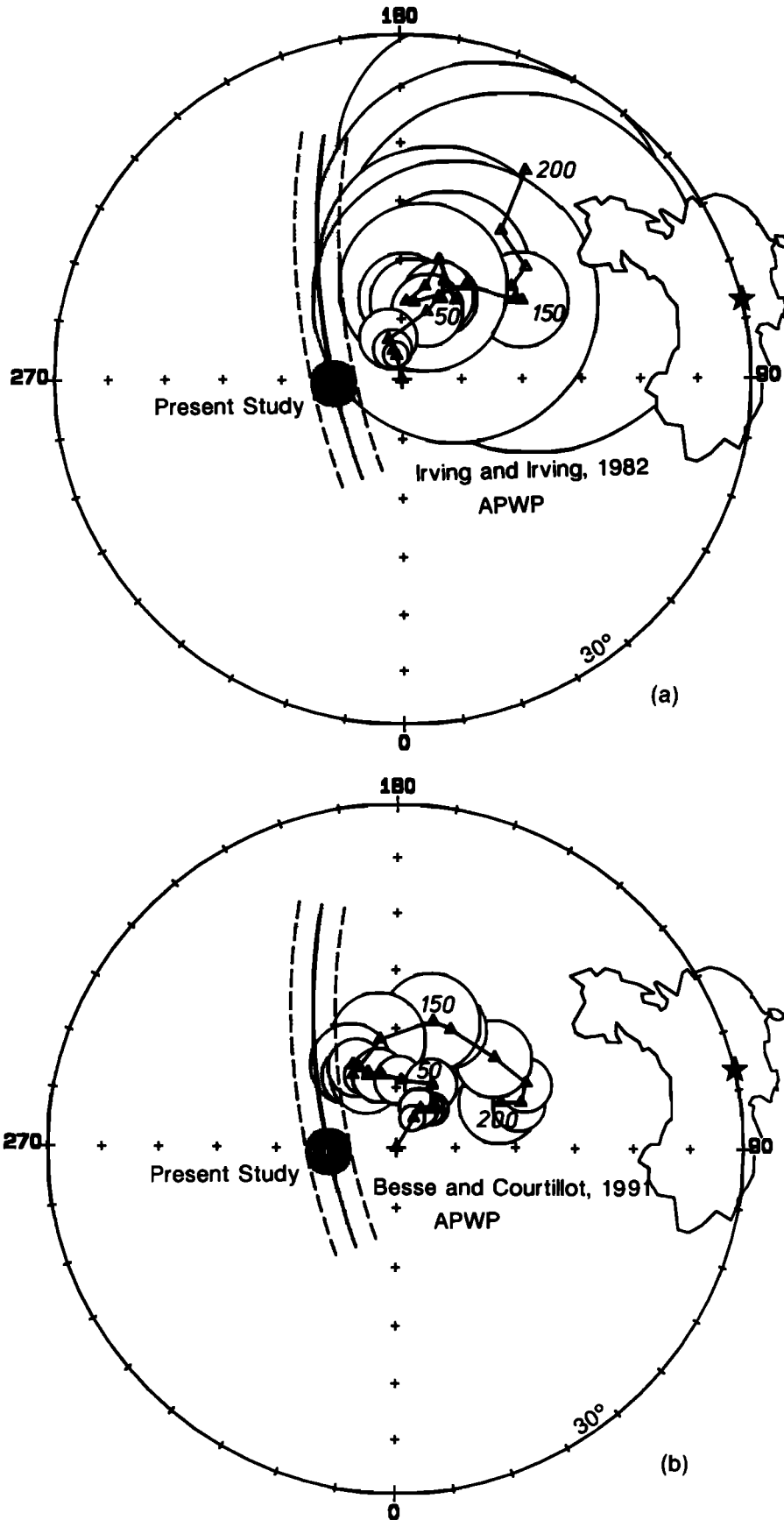


Fig. 19. Apparent polar wander paths for Eurasia, according to (a) Irving and Irving [1982], and (b) Besse and Courtillot [this issue]. The pole from the present study is marked with a shaded circle. The associated small circle centered on the sampling site (star) shows possible pole position on local rotation.

other Cretaceous poles of China (with the exception of the Nanjing pole), but has suffered a  $\sim 15^\circ$  CCW rotation due to local deformation just in front of the Longmen Shan thrust fault. South Sichuan poles have also been rotated CCW, possibly due to deformation by drag along the Red River fault during its left-lateral strike-slip phase [Tapponnier *et al.*, 1986]. Now we will compare the pole with the Eurasian APWP.

Most authors today use the reference Eurasian APWP from Irving and Irving [1982] or Westphal *et al.* [1986]. The new Eurasian APWP of Besse and Courtillot [this issue] differs from the above two mainly in its large hairpin turn during the Jurassic–Cretaceous (Figure 19). At 120 Ma, the Irving and Irving [1982] path is stalled at  $77^\circ\text{N}$ ,  $170^\circ\text{E}$ , while Westphal *et al.* [1986] has a small loop out to  $72^\circ\text{N}$ ,  $190^\circ\text{E}$ . At the same age, the Besse and Courtillot [this issue] curve reaches  $75^\circ\text{N}$ ,  $211^\circ\text{E}$ . While Irving and Irving's [1982] curve predicts that all of Eurasia remained motionless (or had strictly longitudinal motion) during the last half of the Mesozoic, the revised curve tells of a more complex story: in Europe the hairpin turn mostly would be seen as variations in the declination, whereas the variation would be primarily in the inclination of remanence in South-East Asia. Note that while paleomagnetic declination can be lost due to local rotations, the paleoinclination is independent of tectonic rotations, and is therefore inherently more reliable. Thus studies in the far east are critical to confirm this APWP feature.

Because we are interested in the relative motion of South China with respect to stable Eurasia, we plot the paleolatitude expected for Ya'an as if it were rigidly attached to Eurasia (Figure 20). The age limits plotted come from a linear extrapolation of the magnetostratigraphic section, which as we explain above is probably not exact, but is consistent with the paleontological data.

Let us first consider the Irving and Irving [1982] APWP (Figure 20a). Because there is no Mesozoic hairpin turn in this APWP, it would indicate that South China lay at least 1000 km ( $10^\circ$ ) and maybe even 2000 km south of Eurasia at the time of remanence acquisition, regardless of when it occurred. The corresponding collision of South China with Eurasia which must have led to the present configuration can be compared to the 2000 to 3000 km of shortening sustained by the Eurasian craton after the Cenozoic collision with India [e.g., Jaeger *et al.*, 1989]. The creation of the Himalayan Range and the elevation of the Tibetan plateau (not to mention the considerable effects of extrusion of Indochina [Tapponnier *et al.*, 1986]) have no comparable analog to the north of South China. The Qingling Shan, the range which separates North from South China rises only to 3000 m (i.e., less than the average altitude of the Tibetan plateau, 4500 m). Furthermore, the range has Palaeozoic [Mattauer *et al.*, 1985] or at latest Triassic [Sengör, 1984] origins, whereas the red beds we sampled are Jurassic or Cretaceous. While there is major recent strike-slip motion along this range [Peltzer *et al.*, 1985], there does not seem to be enough recent convergence to account for more than 400 km of shortening (P. Tapponnier, personal communication, 1988). There are other foldbelts to the north of the Qingling Shan, but again nothing near the required magnitude. Therefore the Irving and Irving [1982] APWP is not compatible with both the Chinese paleomagnetic data and our present understanding of the geodynamic history of the Chinese blocks.

On the other hand, the Besse and Courtillot [this issue] Eurasian APWP predicts that the sampling region should have had a relatively constant paleolatitude of about  $25^\circ\text{N}$  throughout the Cretaceous (Figure 20b). The observed paleolatitude of Ya'an is also constant, but at  $19^\circ\text{N}$  it is significantly southward of its predicted position, and we must choose between two hypotheses.

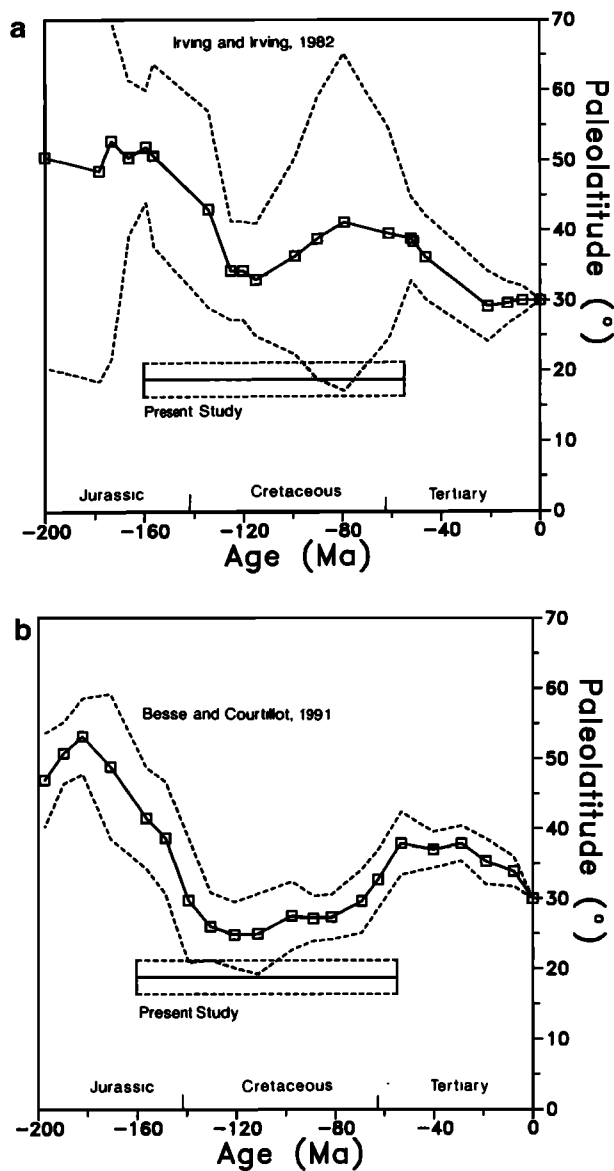


Fig. 20. Paleolatitude of Ya'an according to Eurasian APWP of (a) Irving and Irving [1982], and (b) Besse and Courtillot [this issue]. The paleolatitude found in the present study is given by the light stippled horizontal line, indicating the span in the age of magnetization.

Possibly South China did not accrete onto the Eurasian core until after the period of remanence acquisition, and thus must have done so during the Tertiary. During this period, eastern Eurasia moved about 1000 km northward, so the ensuing convergence was large and should be recognizable, which it is not as we argued above. Reliable Tertiary paleomagnetic poles from China are required to test this possibility.

The hypothesis we prefer is that the sampled period does correspond to the standstill at the tip of the hairpin turn of the revised Eurasian APWP ( $\sim 140$ – $70$  Ma) and that China was fully assembled and attached to Eurasia by this time. The period covered is consistent with the paleontological data, but not the formation ages which reach to the Eocene (40 Ma?). If the start of remanence was actually around 160 Ma (as suggested by a linear extrapolation of the magnetostratigraphic section), we would be forced to accept a late Jurassic collision age for South China onto Eurasia, because of the large difference in paleolatitude at

this time. Unfortunately, there are no reliable early Jurassic poles from China, which would be particularly diagnostic of the age of accretion due to the rapid north-south motion of eastern Eurasia during this period.

The remaining latitude discrepancy during the Cretaceous of about  $600 \pm 300$  km may be indicative of errors in the APWP obtained by transferring poles from other continents onto Europe, but more likely may have been taken up by recent convergence on the Qingling Shan or other foldbelts to the north which separate the Chinese blocks from the rest of Eurasia.

#### CONCLUSION

We have extensively sampled the upper Mesozoic Feixianguan section in the red sandstone Sichuan Basin to place paleomagnetic constraints on the geodynamic history of China and on the Eurasian APWP. While we had expected to find significant apparent polar wander, we discovered a single stable direction throughout the entire 3-km sedimentary section.

This observation raises the worrying possibility of widespread remagnetization (which has been observed in other studies of Chinese paleomagnetism), but we found no indications of this in our results. There is a positive fold test (despite the fact that there are only two sites on one limb of the anticlinal structure). Both polarities are present, and in a section which we sampled at magnetostratigraphic density we were able to propose a correlation with the geomagnetic polarity time scale which is coherent with the (scant) paleontological data. There is an indication that at least some samples contain both magnetite as well as the dominant hematite, and both have recorded the same direction.

Although we have isolated probably the best defined Cretaceous pole in China to date, it is representative of only a small area which must be tied to the rest of the Chinese reference frame by means of a local rotation, which we constrain with the local geology. The resulting pole, at  $70.9^\circ\text{N}$ ,  $225.2^\circ\text{E}$  ( $dp=2.4^\circ$ ,  $dm=6.5^\circ$ ), is coherent with other Cretaceous poles for the Sichuan Basin which we present in an associated paper [Enkin et al., 1991]. The rotation, which is also found on a more regional scale further to the south in Sichuan, is possibly a result of deformation within the South China block during the extrusion of Indochina during the initial phase of the India-Eurasian collision.

All Cretaceous poles from the North China, South China, Tarim and Junggar blocks (except one from Nanjing which we suspect to be significantly more recent in age than the rest) have compatible paleolatitudes which implies that China was fully assembled by this period, although there is evidence of small subsequent rotations.

The Chinese poles are not compatible with the Eurasian APWP of Irving and Irving [1982], which is defined only with Eurasian (largely Siberian) poles and with little data selection, unless a major Tertiary accretion event occurred to the north of South China, for which we see no evidence. Using reliable poles from other continents and transferring them onto Eurasia using ocean kinematics (as Besse and Courtillot [this issue] have done) defines a Mesozoic hairpin turn, with a stable endpoint which lasted the entire Cretaceous. We interpret our pole, and the rest of the Chinese Cretaceous poles as well, to have been magnetized within this period. The remaining discrepancy of a few hundred kilometers must have been taken up north of South China, or possibly indicates a slight error in the Eurasian reference APWP. Lower Jurassic and Tertiary poles from China, which we predict should reveal much higher paleolatitudes, are necessary to confirm our interpretation.

**Acknowledgments.** We thank Elizabeth McClelland of Oxford, Carlo Laj and Piotr Tulcholka of Gif-sur-Yvette and Mansour Bina of St. Maur, and their colleagues for the warm welcome to their laboratories. Paul Tapponnier, Neil Opdyke, Renée Damotte and Yves Gallet helped in discussions and the reading of the manuscript. John Geissman and an anonymous referee greatly improved the article with their detailed reviews. Special thanks are due to Daniel Joseph Wolf for assistance to the first author. A package of programs for PC computers was developed to display and interactively choose and analyze paleomagnetic directions. Their flexibility and ease of use enabled a fuller analysis than is usually performed on paleomagnetic data. These programs are freely available from the first author. This is IGP contribution NS 1120.

#### REFERENCES

- Besse, J., Cinématique des plaques et dérive des pôles magnétiques: Evolution de la Téthys, collisions continentales et couplage noyau-manteau, Doctorat d'Etat thesis, 380 pp., Univ. Paris VII, Paris, 1986.
- Besse, J., and V. Courtillot, Revised and synthetic apparent polar wander paths of the African, Eurasian, North American and Indian plates and true polar wander since 200 Ma, *J. Geophys. Res.*, this issue.
- Burrett, C. F., Plate tectonics and the fusion of Asia, *Earth Planet. Sci. Lett.*, **21**, 181-189, 1974.
- Chan, L. S., C. Y. Wang and X. Y. Wu, Paleomagnetic results from some Permian-Triassic rocks from Southwestern China, *Geophys. Res. Lett.*, **11**, 1157-1160, 1984.
- Chen, Y., and V. Courtillot, Widespread Cenozoic (?) remagnetization in Thailand and its implications for the India-Asia collision, *Earth Planet. Sci. Lett.*, **93**, 113-122, 1989.
- Chen, Y., J.-P. Cogné, V. Courtillot, J. P. Avouac, P. Tapponnier, E. Buffetaut, G. Wang, M. Bai, H. You, M. Li, and C. Wei, Paleomagnetic study of Mesozoic continental sediments along the northern Tien Shan (China) and heterogeneous strain in central Asia, *J. Geophys. Res.*, accepted, 1991.
- Courtillot, V., and J. Besse, Mesozoic and Cenozoic evolution of the North and South China blocks, *Nature*, **320**, 86-87, 1986.
- Cox, A. V., Magnetostratigraphic timescale, in *A Geologic Time Scale*, edited by W. B. Harland, A. V. Cox, P. G. Llewellyn, C. A. G. Pickton, A. G. Smith, and R. Walters, 122 pp., Cambridge University Press, New York, 1982.
- Enkin, R. J., V. Courtillot, L. King, Z. Zhang, Z. Zhuang, and J. Zhang, The stationary Cretaceous paleomagnetic pole of Sichuan (South China Block), *Tectonics*, in press, 1991.
- Fisher, N. I., T. Lewis and B. J. J. Embleton, *Statistical Analysis of Spherical Data*, 329 pp., Cambridge University Press, New York, 1987.
- Holm, E. J., and K. L. Verosub, An analysis of the effects of thermal demagnetization on magnetic carriers, *Geophys. Res. Lett.*, **15**, 487-490, 1988.
- Irving, E., and G. A. Irving, Apparent polar wander paths Carboniferous through Cenozoic and the assembly of Gondwana, *Geophys. Surv.*, **5**, 141-188, 1982.
- Jaeger, J.-J., V. Courtillot and P. Tapponnier, Paleontological view of the ages of the Deccan Traps, the Cretaceous/Tertiary boundary, and the India-Asia collision, *Geology*, **17**, 316-319, 1989.
- Kent, D. V., G. Xu, K. Huang, W. Y. Zhang and N. D. Opdyke, Paleomagnetism of upper Cretaceous rocks from South China, *Earth Planet. Sci. Lett.*, **79**, 179-184, 1986.
- Kent, D. V., X. Zeng, W. Y. Zhang, and N. D. Opdyke, Widespread late Mesozoic to Recent remagnetization of Paleozoic and lower Triassic sedimentary rocks from South China, *Tectonophysics*, **139**, 133-143, 1987.
- Kirschvink, J. L., The least-square line and plane and the analysis of paleomagnetic data, *Geophys. J. R. Astron. Soc.*, **62**, 699-718, 1980.
- Laveine, J. P., Y. Lemoigne, X. Li, X. Wu, S. Zhang, X. Zhao, W. Zhu and J. Zhu, Paleogeography of China in Carboniferous time at the light of paleobotanical data, in comparison with Western Europe Carboniferous assemblages, *C. R. Acad. Sci. Paris*, **304**, 391-394, 1987.
- Lee, G., J. Besse and V. Courtillot, Eastern Asia in the Cretaceous: New paleomagnetic data from South Korea and a new look at Chinese and Japanese data, *J. Geophys. Res.*, **92**, 3580-3596, 1987.

- Li, C., Q. Wang, X. Liu and Y. Tang, Tectonic Map of Asia, Cartographic Publishing House, Beijing, 1982.
- Li, Y., Z. Zhang, M. McWilliams, R. Sharps, Y. Zhai, Y. Li, Q. Li, and A. Cox, Mesozoic paleomagnetic results of the Tarim Craton: Tertiary relative motion between China and Siberia, *Geophys. Res. Lett.*, **15**, 217-220, 1988a.
- Li, Y., M. McWilliams, A. Cox, R. Sharp, Y. Li, Z. Gao, Z. Zhang, and Y. Zhai, Late Permian paleomagnetic pole from dikes of the Tarim Craton, China, *Geology*, **16**, 275-278, 1988b.
- Lin, J., M. Fuller, and W. Zhang, Preliminary Phanerozoic polar wander paths for the North and South China blocks, *Nature*, **313**, 444-449, 1985.
- Lowrie, W., and J. G. Ogg, A magnetic polarity time scale for the early Cretaceous and late Jurassic, *Earth Planet. Sci. Lett.*, **76**, 341-349, 1986.
- Mattauer, M., P. Matte, J. Malavieille, P. Tapponnier, H. Mahuski, Z. Q. Xu, Y. L. Lu and Y. Q. Tang, Tectonics of the Qinling belt: Build-up and evolution of Eastern Asia, *Nature*, **317**, 496-500, 1985.
- McElhinny, M. W., Statistical significance of the fold test in paleomagnetism, *Geophys. J. R. Astron. Soc.*, **8**, 338-340, 1964.
- McElhinny, M. W., B. J. J. Embleton, X. H. Ma, and Z. K. Zhang, Fragmentation of Asia in the Permian, *Nature*, **293**, 212-216, 1981.
- McFadden, P. L. and D. L. Jones, The fold test in palaeomagnetism, *Geophys. J. R. Astron. Soc.*, **67**, 53-58, 1981.
- McFadden, P. L. and M. W. McElhinny, The combined analysis of remagnetization circle and direct observation in paleomagnetism, *Earth Planet. Sci. Lett.*, **87**, 161-172, 1988.
- McFadden, P. L., X. H. Ma, M. W. McElhinny and Z. K. Zhang, Permo-Triassic magnetostratigraphy in China: Northern Tarim, *Earth Planet. Sci. Lett.*, **87**, 152-160, 1988.
- Molnar, P. and P. Tapponnier, Cenozoic tectonics of Asia: Effects of a continental collision, *Science*, **189**, 419-426, 1975.
- Moore, R. C., *Treatise on Invertebrate Paleontology, Part Q, Anthropoda 3, Crustacea, Ostracoda*, Geological Society of America, University of Kansas Press, Kansas City, 1961.
- Opdyke, N. D., K. Huang, G. Xu, W. Y. Zhang, and D. V. Kent, Paleomagnetic results from the Triassic of the Yangtze Platform, *J. Geophys. Res.*, **91**, 9553-9568, 1986.
- Otofuji, Y., Y. Inoue, S. Funahara, F. Murata and X. Zheng, Paleomagnetic study of eastern Tibet -deformation of the Three Rivers region, *Geophys. J. Int.*, **103**, 85-94, 1990.
- Peltzer, G., P. Tapponnier, Z. Zhang and Z. Q. Xu, Neogene and Quaternary faulting in and along the Qingling Shan, *Nature*, **317**, 500-505, 1985.
- Sengör, A. M. C., The Cimmeride Orogenic System and the Tectonics of Eurasia, *Geol. Soc. Am. Spec. Pap.* **195**, 1984.
- Steiner, M., J. Ogg, Z. Zhang and S. Sun, The Late Permian / Early Triassic magnetic polarity time scale and plate motions of South China, *J. Geophys. Res.*, **94**, 7343-7363, 1989.
- Sun, D. Q., and L. B. Wu, Tectonic systems map of the People's Republic of China and adjacent sea area, Cartographic Publishing House, Beijing, 1984.
- Tapponnier, P., and P. Molnar, Active faulting and tectonics in China, *J. Geophys. Res.*, **82**, 2905-2930, 1977.
- Tapponnier, P., G. Peltzer, and R. Armijo, On the mechanism of the collision between India and Asia, *Geol. Soc. Spec. Pub.* **19**, 115-157, 1986.
- Wang, H. Z., Atlas of the Paleogeography of China, Cartographic Publishing House, Beijing, 1985.
- Wang Z., Paleovegetation and plate tectonics: Paleophytogeography of North China during Permian and Triassic times, *Paleoeco., Paleoclim., Paleoeco.*, **49**, 25-45, 1985.
- Westphal, M., M. L. Bazhenov, J. P. Lauer, D. M. Pechersky and J. C. Sibuet, Paleomagnetic implications on the evolution of the tethys belt from the Atlantic Ocean to the Pamirs since the Triassic, *Tectonophysics*, **123**, 37-82, 1986.
- Zhang, Z. M., J. G. Liou and R. G. Coleman, An outline of plate tectonics of China, *Geol. Soc. Am. Bull.*, **95**, 295-312, 1984.
- Zhao, X., A paleomagnetic study of Phanerozoic rock units from Eastern China, Ph.D. thesis, 402 pp., Univ. of Calif., Santa Cruz, 1987.
- Zhao, X., and R. S. Coe, Paleomagnetic constraints on the collision and rotation of North and South China, *Nature*, **327**, 141-144, 1987.
- Zhao, X., and R. S. Coe, Tectonic implications of Permo-Triassic paleomagnetic results from North and South China, in *Deep structure and past kinematics of accreted terranes*, *Geophys. Monogr. Ser./IUGG*, vol.5, edited by J. W. Hillhouse, pp. 267-283, AGU, Washington, D. C., 1989.
- Zhuang, Z. H., D. X. Tian, X. H. Ma, X. F. Ren, X. C. Jiang, and S. J. Xu, A paleomagnetic study along the Ya'an-Tianquan Cretaceous-Eogene Section in Sichuan Basin, *Geophysical and Geochemical Exploration*, **12**, 224-228.
- Zijderveld, J. D. A., A. C. demagnetization of rocks: analysis of results, in *Methods in Paleomagnetism*, edited by D. W. Collinson, K. M. Creer, and S. K. Runcorn, pp. 254-286, Elsevier, New York, 1967.
- R. J. Enkin, Y. Chen, V. Courtillot, and J. Besse, Institut de Physique du Globe de Paris, 4 place Jussieu, 75252 Paris Cedex 05, France.
- L. Xing, Z. Zhang, Z. Zhuang, and J. Zhang, Institute of Geomechanics, Chinese Academy of Geological Sciences, Baiwan Zhuang, Beijing, China.

(Received September 22, 1989;  
revised March 28, 1990;  
accepted April 5, 1990.)